Title

Lineage Tracing Reveals a Subset of Reserve Muscle Stem Cells Capable of Clonal Expansion under Stress

Journal

Cell Stem Cell, 24(6)

ISSN

1934-5909

Authors

Scaramozza, Annarita
Park, Dongsu
Kollu, Swapna
et al.

Publication Date

2019-06-01

DOI

10.1016/j.stem.2019.03.020

Peer reviewed

HHS Public Access

Author manuscript

Cell Stem Cell. Author manuscript; available in PMC 2019 September 06.

Published in final edited form as:

Cell Stem Cell. 2019 June 06; 24(6): 944–957.e5. doi:10.1016/j.stem.2019.03.020.

Lineage Tracing Reveals a Subset of Reserve Muscle Stem Cells Capable of Clonal Expansion under Stress

Annarita Scaramozza[1], **Dongsu Park**[2], **Swapna Kollu**[3], **Isabel Beerman**[4], **Xuefeng Sun**[1], **Derrick J. Rossi**[4,5], **Charles P. Lin**[5,6], **David T. Scadden**[3,4,5], **Colin Crist**[7,8], and **Andrew S. Brack**[1,9,*]

[1]The Eli and Edythe Broad Center for Regenerative Medicine and Stem Cell Research, Department of Orthopedic Surgery, University of California, San Francisco, San Francisco, CA 94143, USA

[2]Department of Molecular and Human Genetics, Baylor College of Medicine, Houston, TX 77030, USA

[3]Center of Regenerative Medicine, Massachusetts General Hospital, Boston, MA 02114, USA

[4]Department of Stem Cell and Regenerative Biology, Harvard University, Cambridge, MA 02138, USA

[5]Harvard Stem Cell Institute, Cambridge, MA 02138, USA

[6]Advanced Microscopy Program, Wellman Center for Photomedicine and Center for Systems Biology, Massachusetts General Hospital, Boston, MA 02114, USA

[7]Lady Davis Institute for Medical Research, Sir Mortimer B. Davis Jewish General Hospital, Montréal, QC H3T 1E2, Canada

[8]Department of Human Genetics, McGill University, Montréal, QC H3A 0C7, Canada

[9]Lead Contact

SUMMARY

Stem cell heterogeneity is recognized as functionally relevant for tissue homeostasis and repair. The identity, context dependence, and regulation of skeletal muscle satellite cell (SC) subsets remains poorly understood. We identify a minor subset of $Pax7^+$ SCs that is indelibly marked by an inducible *Mx1-Cre* transgene in vivo, is enriched for *Pax3* expression, and has reduced ROS (reactive oxygen species) levels. $Mx1^+$ SCs possess potent stem cell activity upon transplantation but minimally contribute to endogenous muscle repair, due to their relative low abundance. In

*Correspondence: andrew.brack@ucsf.edu.

AUTHOR CONTRIBUTIONS

A.S. designed and performed experiments, analyzed data, interpreted results, and wrote the manuscript. D.P. designed and performed experiments, analyzed data, and interpreted results. I.B. and S.K. performed experiments and analyzed data. C.P.L. and D.J.R. designed experiments and edited the manuscript. C.C. performed experiments, analyzed data, and edited the manuscript. D.T.S. conceived the project and edited the manuscript. A.S.B. conceived the project, interpreted experiments, and wrote the manuscript.

SUPPLEMENTAL INFORMATION

Supplemental Information can be found online at https://doi.org/10.1016/j.stem.2019.03.020.

DECLARATION OF INTERESTS

The authors declare no competing interests.

contrast, a dramatic clonal expansion of Mx1^{+} SCs allows extensive contribution to muscle repair and niche repopulation upon selective pressure of radiation stress, consistent with reserve stem cell (RSC) properties. Loss of *Pax3* in RSCs increased ROS content and diminished survival and stress tolerance. These observations demonstrate that the Pax7^{+} SC pool contains a discrete population of radiotolerant RSCs that undergo clonal expansion under severe stress.

Graphical Abstract

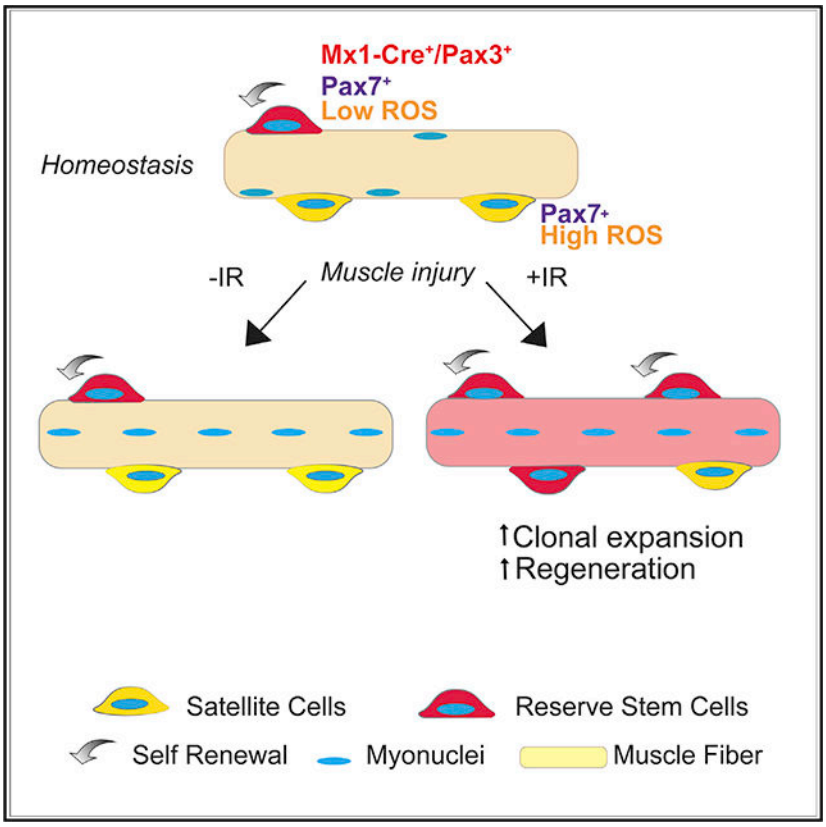

In Brief

Brack and colleagues identify a muscle reserve stem cell population marked by Mx1-Cre and Pax3 within the Pax7^{+} satellite cell pool. After radiation, reserve stem cells clonally expand to become the dominant stem cell population for repair and stem cell maintenance. ROS levels across the satellite cell pool endow radiotolerance.

INTRODUCTION

It is becoming appreciated that stem cell compartments are composed of molecularly and functionally heterogeneous subsets. Cellular heterogeneity within a given pool of stem cells allows for an efficient cellular response under diverse environmental cues. To interrogate functional output of a heterogeneous set of cells requires techniques that can mark and track subsets of cells over time. Lineage tracing is the gold standard approach to determine the

origin and contribution of a specific cell type to tissue development, maintenance, or repair (Kretzschmar and Watt, 2012).

Adult skeletal muscle contains a rare population of quiescent stem cells (satellite cells [SCs]). Lineage tracing studies show that $Pax7^+$ SCs are the cell of origin for muscle regeneration and replenishment of the SC pool (Lepper et al., 2011; Murphy et al., 2011; Sambasivan et al., 2011). Rather than acting as a homogeneous population, SCs are functionally and molecularly heterogeneous (Chakkalakal et al., 2012; Kuang et al., 2007; Rocheteau et al., 2012; Sacco et al., 2008). Based on label dilution assays using a DOX-inducible TetO-H2B-GFP system, the adult SC pool is composed of ~30% label-retaining SCs (LRCs). Transplantation assays reveal that LRCs function as bona fide stem cells, capable of self-renewal and differentiation. Non-label-retaining SCs (nLRCs) are restricted to differentiation, thus functioning as committed progenitors (Chakkalakal et al., 2012, 2014).

In other stem cell compartments, such as intestinal stem cells (ISCs) and hematopoietic stem cells (HSCs), different pools of stem cells are preferentially deployed, depending on the type of injury. In the HSC compartment, distinct subsets favorably seed blood production during homeostatic turnover versus transplantation (Rodriguez-Fraticelli et al., 2018; Sun et al., 2014). In the intestine, lineage tracing and label retention assays show that the intestine contains two populations of stem cells: a radiosensitive, rapidly dividing subset and a rarer, dormant (label-retaining) radiotolerant population, termed a reserve cell (Metcalfe et al., 2014; Montgomery et al., 2011; Tian et al., 2011). The reserve stem cell (RSC) population contributes when the more active and abundant population is damaged. The presence of a molecularly distinct RSC population in other tissues remains enigmatic. Multicolor lineage tracing revealed that the SC population undergoes clonal expansion under the selective pressure of repetitive muscle injuries and during tissue growth (Nguyen et al., 2017; Tierney et al., 2018). The molecular identity of this population remains unknown.

In the present study, we demonstrate that a subset of muscle RSCs are indelibly marked by the *Mx1-Cre* transgene *in vivo* and enriched for *Pax3* expression. We show that $Mx1\text{-}Cre^+$ SCs possess potent stem cell activity under the setting of transplantation and undergo clonal expansion when regenerating injured muscle is exposed to irradiation (IR). *Pax3* is required in RSCs to prevent reactive oxygen species (ROS) accumulation and enable clonal expansion after IR. These findings reveal that stress tolerance is a critical feature governing clonal output and potency within heterogeneous stem cell populations.

RESULTS

Identification of a Subset of SCs Marked by *Mx1-Cre*

In our effort to identify Cre inducible lineage markers to track distinct SC subsets, we examined interferon-inducible *Mx1-Cre* transgenic reporter mice that have been used to detect HSCs, pericytes, and mesenchymal stromal cells (MSCs), muscle resident cells (Dey et al., 2016; Kühn et al., 1995; Park et al., 2012), and epithelial cells (Schneider et al., 2003). Adult uninjured *Mx1-Cre;R26-lsl-eYFP* mice received pIpC (synthetic double-strand RNA to activate *Mx1*) and were left to recover for 14 days (Figure 1A). Quantification of yellow

fluorescent protein (YFP) expression on SCs isolated by fluorescence-activated cell sorting (FACS) or quantified by Pax7 expression on single muscle fibers showed that ~4.5% ± 2% of SCs are *Mx1-Cre* YFP$^+$ (Figure 1A). Consistently, ~5% of SCs were tdTomato$^+$ (tdT) in *Mx1Cre;R26-lsl-tdT* mice; in the absence of pIpC, 0% of SCs were tdT$^+$ (Figure S1A). To examine the myogenic potential of Mx1$^+$ SCs, we sorted and cultured Mx1$^+$ and Mx1$^-$ SCs in growth (high-serum) and differentiating (low-serum) conditions. The majority of Mx1$^+$ and Mx1$^-$ SCs fixed immediately after isolation were Pax7$^+$ (98%). After 2 days in high-serum conditions, over 93% of Mx1$^+$ (n = 1,183 out of 1,259) and Mx1$^-$ (n = 2,681 out of 2,794) SCs were MyoD$^+$ (a marker of activated SCs; Figure 1B) and expanded with similar growth kinetics (Figure S1B). When switched to low serum for 3 days, the majority of Mx1$^+$ and Mx1$^-$ SCs differentiated to form multinucleated myotubes with equivalent fusion indices (Figure S1C). Therefore, Mx1$^+$ and Mx1$^-$ SCs are equally competent to enter the myogenic program and terminally differentiate *in vitro*. Analysis of other Mx1$^+$ populations in skeletal muscle showed co-expression with markers of other cell types, including blood (CD45$^+$), endothelial (CD31$^+$), pericytes and MSCs (Sca1$^+$ and CD105$^+$), and fibro-adipogenic progenitors (FAPs) (Sca1$^+$; Figures S1D–S1H). However, myogenic fate is limited to Mx1$^+$ SCs (Figure S1G). Therefore, *Mx1-Cre* marks multiple cell lineages within skeletal muscle, with intrinsic myogenic potential restricted to Mx1$^+$ SCs.

Although all SCs respond to mitogenic signals, based on a DOX (doxycycline)-inducible *TetO-H2B-GFP* reporter mice that act as a readout of proliferative history, adult muscle is composed of LRCs and nLRCs. LRCs maintain a less-differentiated state during replication and possess greater transplantation potential (Chakkalakal et al., 2012, 2014). To ask whether Mx1$^+$ SCs and LRCs had overlapping properties, we first compared the lineage bias between Mx1$^+$ and Mx1 SCs. Examination of lineage commitment (after 4 days in culture) *in vitro*, based on markers of self-renewal potential (Pax7) and differentiation (myogenin), showed that Mx1$^+$ SCs in comparison to Mx1$^-$ SCs produce progeny that are less differentiated (Figure 1C). These data suggest that Mx1$^+$ and LRCs display similar fate biases.

To make a more direct comparison of the cellular overlap between Mx1$^+$ and LRCs, we crossed *TetO-H2B-GFP* with *Mx1-Cre;R26-lsl-tdT* mice. *Mx1-Cre;R26-lsl-tdT*;*TetO-H2B-GFP* mice were pulsed with DOX from embryonic day 10 (E10) to E16 to induce H2B-GFP expression. LRCs and nLRCs form during postnatal maturation. This was followed by pIpC at 2 months of age to induce the *Mx1-Cre* transgene expression (Figure 1D). In general agreement with our prior work, flow cytometry of freshly isolated adult SCs reveals that 40% of the total adult SC pool is composed of LRCs and 60% of nLRCs (Figure 1E; Chakkalakal et al., 2012, 2014). Comparison of LRC and Mx1$^+$ subsets showed that the Mx1$^+$ fraction is significantly smaller than the LRC population; however, it is enriched within LRCs: ~64% of Mx1$^+$ SCs (3.1% of the 4.5% Mx1$^+$ SC compartment) are within the LRC subset (Figure 1F), suggesting overrep-resentation of Mx1$^+$ SCs within LRCs (Figure 1G).

Transplanted SCs efficiently repopulate the niche and contribute to myofiber repair (Collins et al., 2005; Montarras et al., 2005; Sacco et al., 2008). Our previous work demonstrated that, under the context of transplantation, stem cell potential was restricted to LRCs

(Chakkalakal et al., 2012). That the LRC population is divided into $Mx1^+$ and Mx1 subsets allowed us to examine functional heterogeneity within the LRC population under the context of transplantation. To this end, 3,000 $Mx1^+$ and $Mx1^-$ (LRCs and nLRCs) donor SCs were isolated from *Mx1-Cre;R26-lsl-tdT*;*TetO-H2B-GFP* mice that had received DOX from E10 to E16 and pIpC treated at 2 months of age. The four distinct SC subsets were injected into the injured *tibialis anterior* (TA) muscles of mice (recipient) that had been pre-irradiated (IR) (whole body) and wild-type bone marrow transplanted (WT-BMT). Recipient mice were then given DOX during regeneration to turn on H2B-GFP expression in donor-derived LRCs and nLRCs. Recipient muscles were harvested 30 days after SC engraftment (Figure 1H). Quantitative analysis reveals that LRCs in contrast to nLRCs possess stem cell activity under transplantation conditions, as shown previously in the absence of IR (Chakkalakal et al., 2012). Quantification of the number of donor-derived nuclei and $Pax7^+$ self-renewed SCs on muscle sections showed that $Mx1^+$ LRCs seed approximately 50% more myonuclei compared to $Mx1^-$ LRCs and possess greater self-renewal potential than $Mx1^-$ LRCs (Figures 1I, S1J, and S1K). In contrast, $Mx1^+$ and Mx1 nLRCs displayed negligible contribution to the recipient regenerating muscle, suggesting *Mx1-Cre* expression *per se* does not confer transplantation potential to SCs. Together, these results show that the LRC compartment is composed of two distinct populations defined by *Mx1-Cre*, with the $Mx1^+$ LRCs being more potent.

$Mx1^+$ SCs Retain Stem Cell Potential after Irradiation

Stem cell transplantation is an invaluable assay to determine stem cell activity. However, the assay itself, often coupled with IR to empty the niche, imposes extreme stress on the donor cells. Therefore, the ability of a stem cell to tolerate stress likely confers a functional advantage in this assay. This raises the possibility that the enhanced transplantation potential of $Mx1^+$ SCs is related to enhanced stress tolerance. To this end, we asked whether $Mx1^+$ SCs were able to maintain transplantation potential after IR exposure. We used intravital confocal and 2-photon microscopy to track stem cell engraftment and contribution in the same region of TA muscle tissue over time (Figures 2A and S2A; Lo Celso et al., 2009; Park et al., 2012). SCs from *Actb-Ds-Red* and *Mx1-Cre;R26-lsl-eYFP* mice were used to track the total and Mx1-YFP^+ SC pool, respectively. Ds-Red SCs and $Mx1^+$ SCs were FACS sorted from whole-body IR and non-IR donor mice and transplanted into an injured TA muscle from WT mice (recipients), previously exposed to IR and WT-BMT (Figure 2B). 7 days after transplantation, SCs from *Actb-Ds-Red* and *Mx1-Cre;R26-lsl-eYFP* −IR mice had successfully engrafted. 7 days later, SCs had expanded and aligned with the basal lamina of the recipient muscle fibers. 30 days after transplantation, contribution to myofiber repair was similar between $Mx1^+$ and Ds-Red SCs (Figures 2C, −IR, and 2D). In addition, −IR $Mx1^+$ SCs were able to contribute to muscle fiber differentiation and reoccupy the SC niche (Figures S2B and S2C). Consistent with *in vitro* results (Figure S1G), transplanted $Mx1^+$-$Sca1^+$ FAPs did not engraft and contribute to muscle repair, suggesting that myogenic potential of $Mx1^+$ cells is restricted to SCs *in vivo* (Figure 2E). Therefore, despite their rarity as a fraction of the total SC population *in vivo*, $Mx1^+$ SCs are capable of robust self-renewal and differentiation. Examination of recipient muscle after transplantation of +IR SCs revealed that Ds-Red SCs initially engraft into the muscle but subsequently fail to proliferate (Figures 2C, +IR, and 2D) and contribute to myofiber repair, likely due to an

increase in cell death after IR (Figures S2D–S2F). In contrast, $Mx1^{+}$ SCs retain functionality and are capable of engraftment, expansion, and contribution to myofiber repair (Figures 2C, +IR, and 2D). Therefore, a unique subset of $Pax7^{+}$ SCs marked by *Mx1-Cre* retains stem cell potential after exposure to a lethal dose of IR.

$Mx1^{+}$ SCs Are Radiotolerant

IR limits stem cell survival and function (Blanpain et al., 2011). However, a small subset of muscle progenitors is spared after IR damage (Heslop et al., 2000). We next tested $Mx1^{+}$ SC preservation after exposure to IR. *Mx1-Cre;R26-lsl-eYFP* mice received pIpC every other day for 10 days, followed by a lethal dose of whole-body IR (9 Gy) to target both locally and circulatory contributing cells and a final WT-BMT (Figure 3A). 14 days later, compared to IR controls, +IR mice had a ~40% decline in the total $Pax7^{+}$ SCs pool, whereas the number of $Mx1^{+}$ SC did not change after IR, suggesting that $Mx1^{+}$ SCs are radiotolerant (Figures 3A and S3A). We next analyzed DNA damage markers in freshly isolated $Mx1^{+}$ and $Mx1^{-}$ SCs. Quantification of phosphorylated histone 2AX (γH2AX) (Rogakou et al., 1998; Vahidi Ferdousi et al., 2014) showed that $Mx1^{+}$ SCs formed fewer $\gamma H2AX^{+}$ foci per cell relative to $Mx1^{-}$ SCs both *in vivo* (Figure S3B) and 10 min after IR (2 Gy) exposure *in vitro* (Figure 3B). In addition, the number of DNA strand breaks (DSBs), quantified by comet assay, was less in $Mx1^{+}$ SCs compared to $Mx1^{-}$ SCs (Figure 3B), whereas comet assays performed on FAPs showed a relatively high degree of DSBs after IR, which is independent of the Mx1 lineage (Figure S3C).

DNA damage compromises stem cell fitness. Therefore, tissue-resident stem cells must engage an efficient DNA damage response (DDR) to detect and repair damage or to induce cell death if damage cannot be repaired (Blanpain et al., 2011). In order to test DNA damage response between $Mx1^{+}$ and $Mx1^{-}$ SCs, we performed a comprehensive time course analysis of the DNA damage marker γH2AX on the two SC populations (Figure 3C). The number of $\gamma H2AX^{+}$ foci per cell was lower in $Mx1^{+}$ SCs compared to $Mx1^{-}$ SCs, at all time points analyzed, suggesting that the level of DNA damage was lower in $Mx1^{+}$ SCs. Consistent with the radioprotection properties of $Mx1^{+}$ SCs, LRCs had fewer $\gamma H2AX^{+}$ foci per cell than nLRCs, after IR, although partial overlap was observed (Figure 3D).

Cellular ROS are bi-products of oxidative phosphorylation and regulate stem cell fate decisions (Bigarella et al., 2014). However, over-production in response to radiation stress can induce DNA damage (Ward, 1985). We found that both basal and IR-induced levels of ROS were lower in $Mx1^{+}$ SCs compared to $Mx1^{-}$ SCs (Figure 3E). The difference in ROS between the two populations was greater after IR. Therefore, $Mx1^{+}$ SCs produce fewer free radicals in their quiescent state and in response to exogenous stress.

$Mx1^{+}$ SCs Function as a Reserve Stem Cell Population

RSCs exist within the intestinal stem cell niche; they are rare, dormant, and radiotolerant. During normal tissue turnover, RSC contribution is minor; however, under high stress, such as IR, the dominant proliferative stem cell is ablated, thus liberating the capacity of RSCs to restore tissue homeostasis (Metcalfe et al., 2014; Montgomery et al., 2011; Tian et al., 2011). That $Mx1^{+}$ SCs are rare, enriched within the LRC population, and maintain function

after IR suggests they fulfill at least two of the three criteria of RSCs (Figures 1 and 2). This prompted us to ask whether $Mx1^+$ SC subsets undergo clonal expansion to become the dominant driver of tissue repair after IR stress. To this end, *Mx1-Cre;R26-lsl-eYFP* mice were exposed to IR, WT-BMT, and repeated muscle injuries (Figure 4A). In the absence of IR and injury, muscle fibers lack detectable YFP expression (Figures 4B and 4D), whereas ~5% of the SC pool is $Mx1^+$ (Figure 4E). Thirty days after a primary injury, ~5% of regenerated muscle fibers and ~5% of SCs are Mx1 derived (Figures 4B, 4D, and 4E). After a secondary injury, $Mx1^+$ SCs persisted and gave rise to a small number of regenerating muscle fibers (Figures 4B and 4D). To confirm that the few central-nucleated $Mx1^+$ fibers were derived from proliferating $Mx1^+$ SCs, injured mice were given bromodeoxyuridine (BrdU) in drinking water during a 5-day regeneration assay. Myogenic cells were sorted by FACS, fixed, and stained with a panel of myogenic markers (Pax7, MyoD, and myogenin) and BrdU (Figure S4A). The data showed that 100% of $Mx1^+$ cells were myogenic (data not shown) and had proliferated during regeneration (Figures S4B and S4C). In addition, 40% of $Mx1^+$-derived SCs entered a fusion-competent state, based on the expression of myogenin (Figures S4B and S4C). Therefore, in the absence of IR, $Mx1^+$ SCs possess self-renewal and differentiation potential, with limited contribution to the repair process in their endogenous setting. In contrast, regenerating muscle after IR revealed a significant expansion of proliferating $Mx1^+$ SCs (IR: 65 out of 2,629 $Mx1^+$ SCs out of the total SC pool versus +IR: 438 out of 1,351 $Mx1^+$ SCs out of the total SC pool; Figures S4A and S4B). 30 days after the primary injury, ~65% of regenerating muscle fibers were Mx1-YFP^+ (Figures 4B and 4D). Moreover, the SC pool recovered close to homeostatic levels observed prior to IR and were almost exclusively derived from $Mx1^+$ cells (Figure 4E). After a secondary injury, most newly regenerated fibers (~82%) were YFP^+ derived, thus confirming the extensive self-renewal potential of IR-treated $Mx1^+$ SCs (Figures 4B and 4D). Of note, rare uninjured fibers (lacking central nuclei) in regenerated muscle lack detectable YFP expression (Figure 4C). In the absence of pIpC treatment, there was negligible (<1%) contribution of Mx1-derived cells to muscle repair after IR and injury (Figure 4B). Because the interferon (IFN) activity leading to *Mx1* transgene expression is induced by IR and muscle injury (Cheng et al., 2008), the increased YFP expression after multiple rounds of injury is possibly due to a sequential IFN activation and the induction of *Mx1* transgene expression (Kühn et al., 1995; Velasco-Hernandez et al., 2016). Therefore, we treated *Mx1-Cre;R26-lsl-eYFP* mice with pIpC before and after muscle injury to induce high levels of IFN activity (Figure S4D). Minimal contribution of Mx1-YFP^+ cells to regenerated muscle fibers was observed. Therefore, $Mx1^+$ SCs behave as an RSC population, with minimal contribution during normal regeneration, but in response to IR undergo clonal expansion to replenish the SC pool and regenerating muscle fibers.

Other cell types, such as FAPs, $PW1^+/Pax7^-$ interstitial cells (PICs), and pericytes, may participate in muscle repair (Dellavalle et al., 2011; Joe et al., 2010; Mitchell et al., 2010). Therefore, we tested whether $Pax7^+$ SCs remain the major source for endogenous muscle repair after IR. Adult *Pax7CreER^{TM};R26-lsl-eYFP* mice received tamoxifen (Tmx) for 5 days, followed by IR and WT-BMT reconstitution (Figure S4E). 14 days later, compared to IR controls, +IR mice had ~70% fewer $Pax7^+YFP^+$ SCs (Figures S4E and S4F). In uninjured muscle, YFP expression was restricted to $Pax7^+$ SCs (Figure S4G). 30 days after injury,

100% of regenerated muscle fibers had high levels of YFP expression, independent of IR. Quantification of SC numbers revealed that the $Pax7^{+}YFP^{+}$ pool in regenerated muscle from IR mice returned back to homeostatic levels (Figures S4G and S4H; Shea et al., 2010). After IR, the SC pool increased during repair and repopulated the niche but did not return to homeostatic levels (Figures S4G and S4H). Therefore, $Pax7^{+}$ SCs are responsible for maintenance of the SC pool after IR. Together, these results demonstrate that *Mx1-Cre*$^{+}$/ $Pax7^{+}$ SCs function as a RSC population.

Pax3 Is Required for Stress Tolerance of RSCs

The SC pool is molecularly heterogeneous based on expression of myogenic genes, such as *Pax3*, *Pax7*, and *Myf5* (Kuang et al., 2007; Relaix et al., 2006; Rocheteau et al., 2012). We found that freshly isolated $Mx1^{+}$ SCs and $Mx1^{-}$ SCs have similar levels of *Pax7* and *Myf5*. Interestingly, $Mx1^{+}$ SCs are enriched for *Pax3* (Figure 5A). Pax3 plays a key role during embryonic skeletal myogenesis (Relaix et al., 2005). Pax3 expression undergoes dynamic changes during ontogeny, with the majority of $Pax7^{+}$ SC precursors co-expressing Pax3 during early development, followed by a loss of Pax3 during postnatal maturation, which varies in a muscle-dependent manner (Relaix et al., 2006). Using $Pax3^{GFP/+}$ mice as a readout of $Pax3^{+}$ SCs (Relaix et al., 2005), we showed that the frequency of Pax3-GFP^{+} SCs and $Mx1^{+}$ SCs was similar across different muscle groups. Forelimb and pectoralis muscles contain ~20% Pax3-GFP^{+} and $Mx1^{+}$ SCs; lower limbs contain ~4% (Figures S5A and S5C). The diaphragm contains the highest fraction of Pax3-GFP^{+} and $Mx1^{+}$ SCs (Figure S5A). We find similar expression profiles using Tmx-inducible $Pax3^{tm1.1(cre/ERT2)Lepr}/J$ ($Pax3^{CE/+}$) mice (Southard et al., 2014; Figures S5B and S5D). As further confirmation of the overlap between SC subsets, we quantified *Pax3* mRNA abundance at the single-cell level with RNA-fluorescence *in situ* hybridization (FISH) in SCs from *Mx1-Cre;R26-lsl-eYFP* and *TetO-H2B-GFP* mice. Both $Mx1^{+}$ and LRC SCs had increased *Pax3* expression, based on the number of foci per cell (Figures 5B and S5E). Finally, in quantification of the percentage of SCs expressing detectable levels of *Pax3* mRNA (denoted as 1 foci per cell), we found that the $Pax3^{+}$ population is composed of 58% $Mx1^{+}$ SCs and 71% LRCs (Figure 5C). Together, these data suggest that $Mx1^{+}$ and $Pax3^{+}$ SCs are partially overlapping populations, and both are overrepresented in LRCs.

We next wanted to determine functional overlap between $Mx1^{+}$ and Pax3-GFP^{+} SCs. Similar to $Mx1^{+}$ SCs, Pax3-GFP^{+} SCs displayed lower number of $\gamma H2AX^{+}$ foci per nuclei and DSBs in response to IR, compared to Pax3-GFP SCs (Figures 5D and S5F). Moreover, $Pax3^{CE/+}$-YFP^{+} SCs had lower levels of basal and IR-induced ROS compared to $Pax3^{CE/+}$-YFP SCs (Figure 5E). It was conceivable that pIpC provides a protective effect to stem cells (Velasco-Hernandez et al., 2016). To examine this, we treated $Pax3^{GFP/+}$ mice with pIpC or vehicle. 14 days later, Pax3-GFP^{+} SCs were isolated and exposed to IR. pIpC treatment did not change Pax3-GFP expression or the amount of DNA damage (Figure S5G), suggesting that pIpC does not impact radiotolerance or Pax3-GFP levels. Therefore, $Pax3^{GFP/+}$ marks a pre-existing RSC population. Taken together, we find that the DNA damage response, based on $\gamma H2AX$ at the single-cell level, is skewed within the three SCs subsets, compared to the total SC population. This suggests that radiotolerance operates on a continuum across the SC pool, with $Mx1^{+}$ $Pax3^{+}$ LRCs at one end and $Mx1^{-}$ $Pax3^{-}$ nLRCs at the other (Figure 5F).

To determine whether *Pax3* was required for radiotolerance of RSCs, *Pax3*$^{CE/+}$ mice were crossed with *loxp-Pax3-loxp* (Koushik et al., 2002) and *R26-lsl-tdT* reporter mice to allow for deletion of *Pax3* (*Pax3*$^{CE/f}$) and cell tracking. Mice were injected with Tmx and chased for 14 days, and Pax3^{+} SCs were isolated by FACS. Although *Pax3* was efficiently deleted in Pax3-derived SCs from *Pax3*$^{CE/f}$ compared to *Pax3*$^{CE/+}$ mice after Tmx injection (Figure S5H), the number of SCs was not impacted in uninjured muscle, suggesting that *Pax3* is dispensable for SC maintenance under homeostatic conditions (Figure S5I). Analysis of DNA damage, cellular ROS, and survival reveals that Pax3$^{CE/f}$ SCs have increased DSBs, cellular ROS content, and apoptosis compared to Pax3$^{CE/+}$ SCs in both −IR and +IR conditions (Figures 5G–5I and S5J). Therefore, *Pax3* in RSCs represses free-radical production and DNA damage in response to IR stress.

An imbalance between ROS production and ROS scavenging leads to accumulation of free radicals and increased oxidative stress, which negatively impacts cellular survival. Therefore, ROS levels may mediate the differential response of the SC subsets to IR. We asked whether inhibition of ROS production would decrease DNA damage and increase survival of Pax3^{-} SCs. To this end, FACS sorted Pax3$^{CE/+}$-tdT^{-} and Pax3$^{CE/+}$-tdT^{+} were incubated with or without the antioxidant, N-acetyl-L-cysteine (NAC) 2 h before IR and maintained in NAC for up to 24 h after IR. Compared to vehicle controls, NAC treatment decreased ROS levels (Figure S6A) and the induction of γH2AX^{+} foci per nuclei in Pax3$^{CE/+}$-tdT^{-} after IR (Figure 6A). Therefore, radiotolerance can be acquired through a reduction in ROS levels.

Because *Pax3* is required for radiotolerance and loss of *Pax3* increases cellular ROS content in SCs, we next reasoned that NAC would restore radiotolerance in RSCs lacking *Pax3*. Analysis of DNA damage and apoptosis showed that NAC treatment significantly prevented DNA damage accumulation and apoptosis in Pax3$^{CE/f}$-tdT^{+} SCs (Figure 6B). Therefore, NAC can rescue radiotolerance properties of RSCs lacking *Pax3*.

ROS production is a rapid response to IR, often occurring on the scale of seconds to minutes. Therefore, we next wanted to investigate whether there was a temporal window where ROS levels were critical for radiotolerance. Based on our data, we rationalized that two windows existed: (1) pre-IR, based on basal ROS levels, or (2) within the first hours after IR, based on the initial ROS burst and differential DNA damage markers. First, we pre-treated Pax3$^{CE/+}$-tdT^{-}, Pax3$^{CE/+}$-tdT^{+}, Pax3$^{CE/+}$-tdT^{-}, and Pax3$^{CE/f}$-tdT^{+} SCs with NAC for 2 h, exposed them to IR, and let them recover for either 2 or 24 h. NAC did not prevent accumulation of γH2AX^{+} foci per nuclei at 2 h or apoptosis at 24 h (Figure S6B), suggesting that reducing ROS levels prior to IR is not sufficient to negate its damaging effects. Next, we treated cultures for 4 h (2 h before and 2 h after IR) and left them to recover for 22 h in the absence of NAC. By suppressing the rapid ROS burst after IR, γH2AX^{+} foci per nuclei accumulation was significantly inhibited and survival was improved in Pax3$^{CE/+}$-tdT^{-}and Pax3$^{CE/f}$-tdT^{+} SCs 24 h after IR (Figure 6C). Therefore, inhibition of ROS shortly after IR exposure converts SCs from radiosensitive to radiotolerant.

Finally, we assessed the requirement for *Pax3* on clonal expansion of RSCs under the context of radiation and transplantation. To this end, 3,000 RSCs ($Pax3^{CE/+}$-tdT^{+} and $Pax3^{CE/f}$-tdT^{+}) were isolated from ±IR mice and injected into pre-irradiated, injured muscles of wild-type mice. Muscles from donor recipients were harvested 30 days after SC engraftment (Figure 7A). We find that, in the absence of *Pax3*, IR RSCs lose transplantation potential by ~2-fold. After −IR, RSCs lacking *Pax3* lose transplantation potential by ~10-fold (Figures 7B and 7C). In conclusion, *Pax3* is required for clonal expansion of muscle-resident RSCs.

DISCUSSION

Our studies demonstrate that a molecularly distinct subset of quiescent $Pax7^{+}$ SCs, marked by *Mx1-Cre* and *Pax3*, function as an RSC population characterized by the following criteria: (1) rare; (2) limited contribution under normal tissue maintenance and repair; (3) stress tolerance; and (4) capable of clonal expansion during muscle repair under stress. The relative contribution of this subset depends on the relative fitness of its counterparts (Figure 7D).

The prevailing view of stem cell hierarchies and lineage relationships is that a rarified stem cell sitting at the top of a hierarchy gives rise to all descendants. This has been most convincingly demonstrated in the blood and skeletal muscle system, where a slow dividing subset of stem cells, based on label retention, can reconstitute the stem cell and differentiated progeny after transplantation (Chakkalakal et al., 2012; Foudi et al., 2009). In the present study, we find that the LRC compartment is partitioned into $Mx1^{+}$ and $Mx1^{-}$ subsets, with engraftment and self-renewal potential enriched in the $Mx1^{+}$ fraction. Previous work has demonstrated that subsets of SCs capable of transplantation express high levels of *Pax7* and or bypass *Myf5* during developmental ontogeny (Kuang et al., 2007; Rocheteau et al., 2012). We find equivalent levels of *Pax7* or *Myf5* transcript between $Mx1^{+}$ and $Mx1^{-}$ SCs. This argues that *Mx1-Cre* marks a distinct population from those previously identified. Through the lens of a stem cell hierarchy, the majority of SC and tissue replenishment occurs through a population of $Mx1^{-}$ $Pax3^{-}$ $Pax7^{+}$ SCs. Under conditions of elevated stress, the minor population of $Mx1^{+}Pax3^{+}Pax7^{+}$ SCs is recruited to become the dominant muscle stem cell population. This reveals a level of context-dependent adaptability in the output of cells within a hierarchy (Figure 7D).

A change in the output of one cellular subset, or clone, over another will alter the composition of the stem cell pool and may impact functional diversity. In pathogenic contexts, such as aging and cancer, changes in the clonal complexity (heterogeneity) of cell composition leads to differentiation bias and ineffective drug treatment, respectively (Brooks et al., 2015; Hsu et al., 2018; Sun et al., 2014; Verovskaya et al., 2013). A recent study used a multicolor lineage-tracing approach to quantify $Pax7^{+}$ SC dynamics (Tierney et al., 2018). Whereas clonal diversity was maintained during regeneration from a single injury in adult and aged mice, clonal expansion occurs under the stress of repetitive muscle injuries. This approach cannot determine the molecular identity of such clones. We propose that the expansive $Pax7^{+}$ clone is a $Mx1^{+}$ $Pax3^{+}$ subset. Our results are consistent with the clonal expansion of RSCs due to a decrease in fitness of other clones in response to stress. This

would argue there is feedback between clones that is dependent on the competence for tissue repair. It will be interesting to determine the specific signals that regulate RSC output and the competition between distinct subsets.

RSCs have been unambiguously demonstrated in the intestine (Metcalfe et al., 2014; Montgomery et al., 2011; Tian et al., 2011) and blood (Foudi et al., 2009; Sun et al., 2014; Wilson et al., 2008). The majority of studies examining HSC function have used transplantation as a means to study stem cell potential. A small subset of label-retaining HSCs is endowed with the potential to reconstitute the blood compartment under transplantation and is capable of outcompeting other stem cells within the line-age hierarchy (Foudi et al., 2009; Sun et al., 2014; Wilson et al., 2008). Therefore, intestine, blood, and muscle all contain a discrete subset of stem cells that are adept under stress. This supports the notion that RSCs are a conserved feature across stem cell niches.

We have provided multiple lines of evidence showing the cellular and functional overlap between LRCs, Mx1-Cre^{+}, and Pax3^{+} SCs. Intriguingly, why a subset of SCs marked by IFN-inducible *Mx1-Cre* overlaps with the Pax3 subset remains to be defined. One possible explanation would be that Pax3^{+} SCs are immune competent and able to mount an IFNa response (Pallafacchina et al., 2010). Future experiments are needed to resolve this possibility.

Although *Pax3* expression is diminished in the majority of myogenic cells throughout ontogeny, it is retained in a small subset of adult SCs. Pax3 functions as an important survival factor during embryonic development and postnatal myogenesis (Kassar-Duchossoy et al., 2005; Pani et al., 2002; Relaix et al., 2006; Zalc et al., 2015) and regulates adult SC progenitor migration and differentiation *in vitro* (Boutet et al., 2010). Moreover, Pax3 acts as a transcription factor for Bcl-xL gene, a member of the pro-survival gene family (Margue et al., 2000). We also find that Pax3 is required for stress resistance both in terms of mitogenic and genotoxic stress, consistent with its protective role during development (Zalc et al., 2015). In adult muscle, Pax3^{+} SCs are resistant to environmental stressors (DerVartanian et al., 2019 [this issue of *Cell Stem Cell*]). In the hair follicle, Pax3 is required for melanocyte survival after UV (Yang et al., 2008). Together, these results argue for a generalized protective role of Pax3 and likely explain the ability of RSCs to undergo robust transplantation potential, unarguably a stressful context.

ROS is essential for efficient HSC maintenance in response to external stressors (Ito et al., 2006; Simsek et al., 2010). In the muscle stem cell compartment, microarray analysis of quiescent *Pax3*$^{GFP/+}$ SCs showed an enrichment in genes associated with detoxification and resistance to oxidative stress (Pallafacchina et al., 2010), and treatment of *Pax3*$^{GFP/+}$ SCs with anti-oxidants can regulate fate decisions (L'honoré et al., 2018). Therefore, Pax3^{+}/Mx1^{+} SCs may have a differential metabolic bias compared to the majority of muscle SCs, which switch from mitochondrial fatty acid oxidation to glycolysis during activation (Ryall et al., 2015). If true, this would raise the possibility that other functional differences between Pax3^{+} and Pax3^{-} SCs exist outside of radiotolerance.

It is still under debate why multiple tissues evolve heterogeneous stem cell subsets. One possible explanation is that some cells are more adept at executing specialized functions, which can benefit the tissue or organism. In the context of regeneration after IR, the presence of RSCs allows for tissue homeostasis under contexts of high stress. However, a loss of cellular diversity may lead to adverse outcomes. For example, this population could be a target for oncogenic mutation in response to genotoxic insult. In rhabdomyosarcoma, targeted by the translocation between *Pax3* and *Foxo*, relapse after irradiation occurs in one-third of the population (Smith et al., 2001). Expansion and transformation of radiotolerant cells may be one possible mechanism that leads to generation of cancer stem cells and tumor relapse. This would be consistent with cancer stem cells having low ROS levels and being more resistant to radiation therapy (Diehn et al., 2009). This suggests that radiotolerant RSCs can act as "friend and foe."

Based on lineage tracing and functional analysis, we have provided an unambiguous demonstration of a discrete reserve muscle stem cell population that is mobilized under conditions of high stress. The identification of markers and regulators of functionally distinct stem cells within a given niche will help to determine the molecular mechanisms that maintain stem cell heterogeneity during development, regeneration, and disease.

STAR★METHODS

CONTACT FOR REAGENT AND RESOURCE SHARING

Further information and requests for reagent and resources should be directed to the Lead Contact, Andrew S. Brack (andrew.brack@ucsf.edu).

EXPERIMENTAL MODEL AND SUBJECT DETAILS

Animals—All animal work was in accordance with the animal ethics committee at University California of San Francisco. Mice were housed in a pathogen-free barrier facility, under a 14-hour light / 10-hour dark cycle and temperature-controlled environment with standard diet and water *ad libitum*. *C57BL/6*, *B6.Cg-Tg(Mx1-cre)1Cgn/J (Mx1-Cre)*, *Pax3$^{tm1.1(cre/ERT2)Lepr}$/J (Pax3$^{CE/+}$)*, *B6.129X1-Gt(ROSA)26Sor$^{tm1(EYFP)Cos}$/J* (*R26-lsl-eYFP*), *B6.Cg-Gt(ROSA)26Sortm9(CAG-tdTomato)Hze/J (R26-lsl-tdT)* and *Actb-DsRed.T3* mice were purchased from Jackson Laboratory. *Pax7-CreER^{TM}*, *Pax3$^{GFP/+}$*, *loxp-Pax3-loxp (l-Pax3-l)*, *TetO-H2B-GFP* mice were a gift from C. Keller (Nishijo et al., 2009), C. Crist (Relaix et al., 2005), S. Conway (Koushik et al., 2002) and H. Hock (Foudi et al., 2009) respectively. *Mx1-Cre, R26-lsl-eYFP, R26-lsl-tdT and TetO-H2B-GFP* were used to generate *Mx1-Cre;R26-lsl-eYFP, Mx1-Cre-R26-lsl-tdT and Mx1-Cre-R26-lsl-tdT;TetO-H2B-GFP*, respectively. *Pax7-CreER^{TM} and R26-lsl-eYFP* were crossed to generate *Pax7-CreER^{TM};R26-lsl-eYFP. Pax3$^{CE/+}$, R26-lsl-eYFP, R26-lsl-tdT and loxp-Pax3-loxp* were crossed to generate *Pax3$^{CE/+}$-R26-lsl-eYFP, Pax3$^{CE/+}$-R26-lsl-tdT, Pax3$^{CE/f}$-R26-lsl-eYFP, Pax3$^{CE/f}$-R26-lsl-tdT*. Both male and female adult mice (2–3 months) were used. All animals were maintained on a *C57BL/6J* background. All the animals were not involved in any previous procedures.

Primary mouse myogenic cells *in vitro* culture—For plated murine SC cultures, cells were FACS isolated from adult mice and seeded onto pre-coated ECM gel (Sigma) dishes and expanded in either growth media (GM) with 20% Fetal bovine serum (FBS) and 5 ng ml^{-1} FGF2, plating media (PM) with 10% HS, DMEM, or induced to differentiate in differentiation media (DM) with 2% HS, DMEM for 72 hours. N-Acetyl Cysteine (Sigma) was used at 10mM in FACS rinsing media (10% HS, in Ham's F-10) and GM.

METHOD DETAILS

Animal procedures—Tamoxifen (Tmx) was resuspended in corn oil at 20 mg/ml and administered daily at 150 mg/kg body weight via intraperitoneal (i.p.) injection in adult mice for 5 days. Polyinosinic–polycytidylic acid sodium salt (pIpC) was resuspended in water at 2 mg/ml and administered every 48 hours for 10 days at 25mg/kg body weight. For H2B-GFP expression in transplanted satellite cells (SCs) from *Mx1-Cre-R26-lsl-tdT;TetO-H2B-GFP*, doxycycline (Dox) was dissolved in drinking water (2mg/ml) supplemented with 5% of sucrose. For embryonic H2B-GFP expression, pregnant females were injected at E10.5 with Dox (150 μl at 1 mg/ml) and immediately switched to drinking water containing Dox (2 mg/ml) until E16.

For *in vivo* proliferation assay during skeletal muscle regeneration, bromodeoxyuridine (BrdU) was dissolved in drinking water (2mg/ml) supplemented with 5% of sucrose. Brdu water was given to *Mx1-Cre;R26-lsl-eYFP* mice continuously for 5 days after muscle injury.

Prior to skeletal muscle injury, bone marrow transplantation and SC transplants mice were anesthetized by 1%–4% l/min O_2 isoflurane inhalation.

For muscle injury, the *tibialis anterior* (TA) and *extensor digitorum longus* (Foudi et al., 2009) muscles were poked 24 times before injecting 50 μL barium chloride ($BaCl_2$) suspended in PBS (1.2% w/v, Sigma) in several locations to homogenously distribute the solution throughout both muscles.

Total body mouse irradiation was performed by using a cobalt irradiator within one of the barrier facilities. Mice were placed into a rotating pie-shaped holder (to limit mobility and insure equal irradiation), which is then secured in the irradiator to deliver a dose of 9 Gy. Mice are monitored to assure there is no acute illness. Irradiated mice were injected within 24 hours with *C57/BL6* donor bone marrow cells (1×10^6) in 50 μL of sterile phosphate buffered saline (PBS) via retro-orbital injection. For a 24Gy local irradiation mice were anesthetized and shielded in order that only one lower limb was exposed to the source of radiation.

For transplantation experiments, Mx1-Cre^+YFP^+ (Mx1-YFP^+Vcam^+/Int-$a7^+$/$CD45^-CD31^-$/$Sca1^-$), $DsRed^+$ ($DsRed^+Vcam^+$Int-$a7^+CD45^-CD31^-$/$Sca1^-$) SCs (3000/mouse) or Mx1-YFP^+Sca1^+ fibroadipogenic progenitors (FAPs) or pericytes (Mx1-YFP^+/$Sca1^+$/$CD105^+$) were FACS purified from 14 days post-irradiated or non-irradiated *Mx1-Cre;R26-lsl-eYFP* and *Actb-DsRed.T3* mice. $Mx1^+$ and $Mx1^-$ LRC and $Mx1^+$ and $Mx1^-$ nLRC were FACS sorted from non-irradiated *Mx1-Cre-R26-lsl-tdT;TetO-H2B-GFP*, mice. All Sorted SCs and FAPs (3000/mouse) were injected into TA muscle of *C57BL/6* mice that had been whole

body irradiated (9Gy) and wild-type bone marrow reconstituted two weeks before transplantation and injured 1.5-days before with 1.2% $BaCl_2$ (Sigma). For Pax3 transplantation experiments, $Pax3^{CE/+}$-tdT^+ and $Pax3^{CE/f}$-tdT^+ SCs were FACS purified from 14d post locally irradiated (24Gy) or non-irradiated *$Pax3^{CE/+}$-R26-lsl-tdT* and *$Pax3^{CE/f}$-R26-lsl-tdT* donor mice. Sorted SCs (3000/mouse) were injected into TA muscle of *C57BL/6* mice that had been locally irradiated (24Gy) two weeks prior transplantation and injured 1.5 days before transplantation.

Flow cytometry analysis and FACS—Skeletal muscle tissue from hindlimb, forelimb and pectoralis, diaphragm muscles were dissected, gently minced with scissors and digested with 0.2% of Collagenase II in DMEM for 90 minutes in shaking water bath at 37°C.

Digested tissue then was washed twice with rinsing media (10% HS, in Ham's F-10) and spinned at 1500 rpm at 4°C for 5 minutes. Second digestion was then performed by adding Collagenase II (0.2%) and Dispase (0.4%) in rinsing media for 30 minutes in shaking water bath at 37°C. Digested tissue was then passed through a 20-gauge needle and 10 mL syringe for three times and filtered through a 40 μm filter and spin at 1500 rpm at 4°C for 5 min. A second filter step was done though a 20 μm filter followed by centrifuge at 1500 rpm at 4°C for 5 min, to generate a single cell suspension ready for antibody staining.

Digested tissue was stained using the following antibodies: 1:100 VCAM1-PE (Invitrogen) or 1:100 biotin-conjugated anti-VCAM1 (Novus), 1:250 integrin-α7–649 (AbLab), 1:250 CD31-PE/Cy7 (BD Biosciences), 1:250 CD45-PE/Cy7 (BD Biosciences), and 1:250 Sca1-APC/Cy7 (BD Biosciences). Cells were incubated with primary antibodies for 45 min on ice, washed with cold rinsing buffer and then incubated with 1:100 streptavidin-brilliant violet 421 (BioLegend) and the remaining conjugated antibodies for a further 30 min. Propidium Iodide (Rogakou et al., 1998), 7-Aminoactinomycin D (7-AAD) were used for viable cell gating. Myogenic cells had the following profile: $VCAM1^+$/integrin-$a7^+$/$CD31^-$/$CD45^-$/$Sca1^-$/PI^- ($7AAD^-$). To analyze and sort $Mx1^+$ non-myogenic mesenchymal cells, mononucleated cells from muscle were stained with 1:100 CD105-PE (BioLegend) or 1:100 CD140a-PE (BioLegend) in combination with VCAM1-Brilliant Violet 421, Integrin-α7–649, CD31- and CD45-PE/Cy7 and Sca1-APC/Cy7 antibodies. Flow cytometric analysis and sorting were performed using FACS-Aria II (BD Biosciences).

Single muscle fiber *ex vivo* culture—Viable single myofibers were isolated from the extensor digitorum longus (Foudi et al., 2009) muscle of 2–3 months old mice following dissociation with collagenase I solution (0.2%) for 1.5 hours at 37°C. Dissociated single myofibers were manually collected and purified under a dissection microscope, then either fixed in suspension immediately in 4% paraformaldehyde (PFA) for 10 min or maintained in suspension culture for 48 h with plating media (PM) composed of Dulbecco's Modified Eagle's Medium (DMEM) and 10% horse serum (HS).

Immunofluorescent staining and microscopy—For plated SCs, 8 well Permanox® chamber slides (Nunc®Lab-Tek®) or black-walled 96 well plates were used and cells fixed with 4% (PFA) for 10 minutes. Following fixation, material was permeabilized with 0.2% Triton X-100, in Phosphate Buffer Saline (PBS) (PBS-TX) solution for 10 minutes and then

blocked with 10% goat serum in PBS-TX for 30 minutes to reduce nonspecific antibody binding. Cells were then incubated with the following antibodies at 4°C overnight: mouse anti-Pax7 (1/100, DSHB), rabbit anti-myogenin (1/250, Santa Cruz), rabbit anti-MyoD (1/70, Santa Cruz), rabbit anti-MHC (1/500, Sigma Aldrich), rabbit anti-γH2AX (1/500, Cell Signaling), rabbit anti-Caspase3 (1/500, Cell Signaling), rat anti-Brdu (1/500, Abcam), rabbit anti-Ki67 (1/500, Abcam) chicken anti-laminin (1/5,000, Abcam), rabbit anti-laminin (1/500 Abcam), rabbit anti-GFP (1/500, Thermo Fisher), chicken anti-GFP (1/500, Aves). Corresponding species-specific Alexa-conjugated (488, 546, 594, 647) secondary antibodies (Thermo Fisher) and 100 ng/ml of DAPI (4,6-diamidino-2-phenylindole; Vector Laboratories) were used at 1/2000 for immunohistochemistry and applied for 1h at room temperature. For Brdu detection, following fixation, cells were washed with PBS and then incubated 20 minutes in sodium citrate 10mM, preheated at 95°C−100°C. Cells were then cooled down in citrate buffer for 20 minutes and stained for Brdu, GFP and Myogenic markers, following the staining method described above. Cellular senescence assay (EMD Millipore) and TUNEL Andy Fluor 647 apoptosis detection kit (GeneCopoeia) were performed according to the manufacturer's recommendations. Images were processed with Nikon NID-elements software.

Multiplex *in situ* hybridization with RNAscope—For *in situ* hybridization experiments, FACS sorted SCs were plated on 8 well Permanox® chamber slides (Nunc®Lab-Tek®) and immediately fixed with 4% PFA for 30min at 4°C before being processed for RNA *in situ* detection for *Pax3* using RNAscope Multiplex Fluorescent Reagent Kit v2 (Advanced Cell Diagnostics) according to the manufacturer's instructions for cultured adherent cell. Probe used was Mm-Pax3-C2 (cat# 455801-C2). After RNA detection, sections were co-stained for GFP and Pax7 protein using rabbit anti-GFP and mouse ant-Pax7 primary antibodies. For *Pax3* detection a secondary antibody, with TSA plus Cy5 was used for fluorescent signal amplification (NEL745E001KT, PerkinElmer, 1:1000). Corresponding species-specific Alexa-conjugated (488, 546) secondary antibodies (Thermo Fisher) were used for GFP and Pax7 staining. Nuclei were visualized using DAPI (1.0 μl/ml). Z stacks images were acquired on a Leica DMi8 Confocal using a 63x objective.

Intravital microscopy—To image myogenic differentiation of transplanted SCs *in vivo*, indicated mice were anesthetized and prepared for a custom-built intravital microscope specifically designed for live animal imaging as described previously (Sipkins et al., 2005; Park et al., 2012). All mice except Ds-Red SC-transplanted mice were injected retro-orbitally with 20 μL of non-targeted Q-dot 705 (Thermo Fisher) diluted in 80 μL of PBS. To expose injured TA muscle, a small incision (~1 cm) was made in lateral hind limb skin covering TA muscle. After the mouse was mounted on a 3 axis motorized stage (Sutter MP385), the TA muscle was scanned for second harmonic generation (SHG by femto-second titanium:sapphire laser pulses: 880 nm) from bones and Q-dot signals (633 nm excitation, 650−760 nm detection) from vasculature to identify the myofibers of TA muscle and the lateral tibia head as a landmark. YFP-(492 nm excitation, 520 nm detection) or DsRed-expressing SCs and myofibers (532 nm excitation, 590 nm detection) were simultaneously imaged by confocal microscopy. To trace the muscle formation by transplanted SCs, the injured TA muscle was mapped by 4 to 6 consecutive images (660

μm^2/image), which covered most of the TA muscle. All images were recorded with their distance to the tibia head, to define their precise location. Each image was recorded by Z stacks with 50−100 μm depth from muscle surface and 2 μm interval. After *in vivo* imaging, the skin was re-closed using a VICRYL plus suture (Ethicon), and post-operative care was provided. 3-D Images were reconstructed using Nikon NIS-Elements software, and relative fluorescence signal intensity was measured by ImageJ software.

Histology and Immunofluorescence—TA muscles were dissected and post-fixed in 4% PFA for 30min on ice. For immunohistochemistry, whole muscles were embedded in OCT, frozen and cryosectioned onto glass slides. Before, Pax7 staining, slides underwent blocking with 1:10 MOM (Vectors lab) in 10% Goat Serum, 0.2% PBS-TX and then incubated with the following antibodies overnight at 4°C, 1:20 mouse Pax7 (DSHB), 1:500 chicken GFP (Aves) and 1:500 rabbit anti-Laminin (Abcam, ab11575). Bridge 1:500 rat anti-mouse (AbD Serotec, MCA 336) in PBS-10%Goat Serum was applied for 40 min at room temperature, followed by species-specific fluorochrome-conjugated secondary antibodies (Invitrogen) for 1h at room temperature, before being mounted with 100 ng/ml of Dapi (4,6-diamidino-2-phenylindole; Vector Laboratories). Confocal Images were acquired with a Nikon Eclipse Ti epifluorescence microscope equipped with a Q-imaging Micropublisher digital CCD color camera. Images were processed with Nikon NID-elements software.

Analysis of satellite cells *in vivo*—Muscles sections were stained with anti-Pax7, anti-GFP and anti-laminin, to determine the number of Pax7-YFP$^+$, Pax7$^+$Mx1-YFP$^-$ and Pax7$^+$Mx1-YFP$^+$ SCs or the number of Pax7$^+$H2BGFP$^+$Mx1tdt$^+$ underneath the basal lamina (anti-laminin). The total number of Pax7-YFP$^+$, Pax7$^+$Mx1-YFP$^-$, Pax7$^+$Mx1-YFP$^+$ and Pax7$^+$H2BGFP$^+$Mx1tdt$^+$ cells was quantified in a minimum of five to ten serial sections per muscle in three separate regions from the mid-belly of the muscle. The number of Pax7-YFP$^+$, Pax7$^+$Mx1-YFP$^-$ and Pax7$^+$Mx1-YFP$^+$ cells was quantified on freshly isolated single EDL muscle fibers. A minimum of 20−30 muscle fibers were counted per animal.

Irradiation *in vitro*, DNA damage analysis and Comet Assay—FACS sorted SCs were plated in eight-well Permanox® chamber slides (Nunc®Lab-Tek®) and irradiated with 2Gy then fixed with 4% PFA at different time point after IR. Myogenic cells were stained with anti-Pax7, anti-GFP, anti-γH2AX and DAPI. Z stacks images were acquired on a Leica DMi8 Confocal using a 63x objective and maximum projection images were analyzed for manual quantification of γH2AX. Quantification of three experiments was performed in triplicate and 200−300 cells were counted per condition. To assess cell growth, SCs were plated (500 cells per well, Nunc eight-well Permanox chamber slides) and the number of cells present in each individual well was determined every day for 5–6 days in culture (20%FBS, F10). Alkaline comet assays were performed using Trevigen CometAssay® kits and slides according to the manufacturer's protocol. Briefly, FACS sorted SCs were embedded in Comet LMAgarose and transferred onto Trevigen HTCometSlides. The immobilized cells were lysed overnight and treated with freshly made alkaline unwinding solution followed by electrophoresis in alkaline conditions using Trevigen's CometAssay® Electrophoresis System. Cells were stained with Sybr® Gold and imaged. Analysis was

performed on blinded files using CometScore (TriTek Corp) where values for percent tail DNA and Olive moment were generated. Statistical significance was calculated in Prism (GraphPad) utilizing the Mann-Whitney test.

CELL ROX assay *in vitro*—FACS sorted SCs were exposed to 2Gy irradiation or not and resuspended in rinsing media containing CellROX® reagents (Thermo-fisher) at final concentration of 5uM. Cells were then immediately plated on eight-well Permanox® chamber slides (Nunc® Lab-Tek®) and incubated for 30 minutes at 37°C. Media was removed, cells were gently washed for 3 times with PBS and counterstained with DAPI. Cells were immediately imaged for CellROX® fluorescence intensity with a 40x objective using a Nikon Eclipse Ti.

RNA isolation and RT-qPCR—RNA extraction from FACS sorted SCs was performed using TRIZOL® protocol. RT-qPCR was performed on a Step One Plus Real Time PCR machine (Applied Biosystems) and ViiA7 by Life Technologies (Applied Biosytems) with Platinum SYBR Green qPCR SuperMix-UDG and ROX master mix (Invitrogen) using primers against *Pax7, Myf5, GAPDH, Pax3*. All reactions for RT-qPCR were performed using the following thermal cycler conditions: 50°C for 2 min, 95°C for 2 min, 40 cycles of a two-step reaction, denaturation at 95°C for 15 s, annealing at 60°C for 30 s. Data are from three separate reactions performed in triplicate from n = 3−5 mice.

Image processing and quantification—All images were composed, edited and modifications applied to the whole image using NES, LAS AF and Photoshop CS6 (Adobe).

QUANTIFICATION AND STATISTICAL ANALYSIS

All results are presented as mean ± standard error of the mean (SEM) or standard deviation (SD) where indicated. Statistical analysis was performed using either a Student’s t tests or Mann-Whitney test to calculate differences between two groups and either one-way or two-way ANOVA with post hoc test for multiple comparisons (Graphpad Prism®; version 7). Sample size and/or replicate number for each experiment are indicated in the figure legends. Results with p values of less than 0.05 were considered statistically significant.

Supplementary Material

Refer to Web version on PubMed Central for supplementary material.

ACKNOWLEDGMENTS

We thank all the staff at HCSI-CRM Flow Cytometry Core Facility (MGH) and at Parnassus Flow Cytometry core (UCSF). We thank S. Eliazer, K. Chui, R. Gomez, S. Jamet, A. Orthwein, and K. Asiev for sharing advice and expertise. This work was supported by NIH grants RO1 060868 to A.S.B. and NIH U01 HL100402 to D.T.S. and C.L.

REFERENCES

Bigarella CL, Liang R, and Ghaffari S (2014). Stem cells and the impact of ROS signaling. Development 141, 4206–4218. [PubMed: 25371358]

Blanpain C, Mohrin M, Sotiropoulou PA, and Passegué E (2011). DNA-damage response in tissue-specific and cancer stem cells. Cell Stem Cell 8, 16–29. [PubMed: 21211780]

Boutet SC, Biressi S, Iori K, Natu V, and Rando TA (2010). Taf1 regulates Pax3 protein by monoubiquitination in skeletal muscle progenitors. Mol. Cell 40, 749–761. [PubMed: 21145483]

Brooks MD, Burness ML, and Wicha MS (2015). Therapeutic implications of cellular heterogeneity and plasticity in breast cancer. Cell Stem Cell 17, 260–271. [PubMed: 26340526]

Chakkalakal JV, Jones KM, Basson MA, and Brack AS (2012). The aged niche disrupts muscle stem cell quiescence. Nature 490, 355–360. [PubMed: 23023126]

Chakkalakal JV, Christensen J, Xiang W, Tierney MT, Boscolo FS, Sacco A, and Brack AS (2014). Early forming label-retaining muscle stem cells require p27kip1 for maintenance of the primitive state. Development 141, 1649–1659. [PubMed: 24715455]

Cheng M, Nguyen MH, Fantuzzi G, and Koh TJ (2008). Endogenous interferon-gamma is required for efficient skeletal muscle regeneration. Am. J. Physiol. Cell Physiol. 294, C1183–C1191. [PubMed: 18353892]

Collins CA, Olsen I, Zammit PS, Heslop L, Petrie A, Partridge TA, and Morgan JE (2005). Stem cell function, self-renewal, and behavioral heterogeneity of cells from the adult muscle satellite cell niche. Cell 122, 289–301. [PubMed: 16051152]

Dellavalle A, Maroli G, Covarello D, Azzoni E, Innocenzi A, Perani L, Antonini S, Sambasivan R, Brunelli S, Tajbakhsh S, and Cossu G (2011). Pericytes resident in postnatal skeletal muscle differentiate into muscle fibres and generate satellite cells. Nat. Commun 2, 499. [PubMed: 21988915]

DerVartanian A, Quetin M, Michineau S, Aurade F, Hayashi S, Dubois C, Rocancourt D, Drayton-Libotte B, Szegedi A, Buckingham M, et al. (2019). PAX3 confers functional heterogeneity in skeletal muscle stem cell responses to environmental stress. Cell Stem Cell 24 Published online April 18, 2019. 10.1016/j.stem.2019.03.019.

Dey D, Bagarova J, Hatsell SJ, Armstrong KA, Huang L, Ermann J, Vonner AJ, Shen Y, Mohedas AH, Lee A, et al. (2016). Two tissue-resident progenitor lineages drive distinct phenotypes of heterotopic ossification. Sci. Transl. Med 8, 366ra163.

Diehn M, Cho RW, Lobo NA, Kalisky T, Dorie MJ, Kulp AN, Qian D, Lam JS, Ailles LE, Wong M, et al. (2009). Association of reactive oxygen species levels and radioresistance in cancer stem cells. Nature 458, 780–783. [PubMed: 19194462]

Foudi A, Hochedlinger K, Van Buren D, Schindler JW, Jaenisch R, Carey V, and Hock H (2009). Analysis of histone 2B-GFP retention reveals slowly cycling hematopoietic stem cells. Nat. Biotechnol 27, 84–90. [PubMed: 19060879]

Heslop L, Morgan JE, and Partridge TA (2000). Evidence for a myogenic stem cell that is exhausted in dystrophic muscle. J. Cell Sci 113, 2299–2308. [PubMed: 10825301]

Hsu JI, Dayaram T, Tovy A, De Braekeleer E, Jeong M, Wang F, Zhang J, Heffernan TP, Gera S, Kovacs JJ, et al. (2018). PPM1D mutations drive clonal hematopoiesis in response to cytotoxic chemotherapy. Cell Stem Cell 23, 700–713.e6. [PubMed: 30388424]

Ito K, Hirao A, Arai F, Takubo K, Matsuoka S, Miyamoto K, Ohmura M, Naka K, Hosokawa K, Ikeda Y, and Suda T (2006). Reactive oxygen species act through p38 MAPK to limit the lifespan of hematopoietic stem cells. Nat. Med 12, 446–451. [PubMed: 16565722]

Joe AW, Yi L, Natarajan A, Le Grand F, So L, Wang J, Rudnicki MA, and Rossi FM (2010). Muscle injury activates resident fibro/adipogenic progenitors that facilitate myogenesis. Nat. Cell Biol 12, 153–163. [PubMed: 20081841]

Kassar-Duchossoy L, Giacone E, Gayraud-Morel B, Jory A, Gomès D, and Tajbakhsh S (2005). Pax3/Pax7 mark a novel population of primitive myogenic cells during development. Genes Dev. 19, 1426–1431. [PubMed: 15964993]

Koushik SV, Chen H, Wang J, and Conway SJ (2002). Generation of a conditional loxP allele of the Pax3 transcription factor that enables selective deletion of the homeodomain. Genesis 32, 114–117. [PubMed: 11857794]

Kretzschmar K, and Watt FM (2012). Lineage tracing. Cell 148, 33–45. [PubMed: 22265400]

Kuang S, Kuroda K, Le Grand F, and Rudnicki MA (2007). Asymmetric self-renewal and commitment of satellite stem cells in muscle. Cell 129, 999–1010. [PubMed: 17540178]

Kühn R, Schwenk F, Aguet M, and Rajewsky K (1995). Inducible gene targeting in mice. Science 269, 1427–1429. [PubMed: 7660125]

L'honoré A, Commère PH, Negroni E, Pallafacchina G, Friguet B, Drouin J, Buckingham M, and Montarras D (2018). The role of Pitx2 and Pitx3 in muscle stem cells gives new insights into P38a MAP kinase and redox regulation of muscle regeneration. eLife 7, e32991. [PubMed: 30106373]

Lepper C, Partridge TA, and Fan CM (2011). An absolute requirement for Pax7-positive satellite cells in acute injury-induced skeletal muscle regeneration. Development 138, 3639–3646. [PubMed: 21828092]

Lo Celso C, Fleming HE, Wu JW, Zhao CX, Miake-Lye S, Fujisaki J, Côté D, Rowe DW, Lin CP, and Scadden DT (2009). Live-animal tracking of individual haematopoietic stem/progenitor cells in their niche. Nature 457, 92–96. [PubMed: 19052546]

Margue CM, Bernasconi M, Barr FG, and Schäfer BW (2000). Transcriptional modulation of the anti-apoptotic protein BCL-XL by the paired box transcription factors PAX3 and PAX3/FKHR. Oncogene 19, 2921–2929. [PubMed: 10871843]

Metcalfe C, Kljavin NM, Ybarra R, and de Sauvage FJ (2014). Lgr5+ stem cells are indispensable for radiation-induced intestinal regeneration. Cell Stem Cell 14, 149–159. [PubMed: 24332836]

Mitchell KJ, Pannérec A, Cadot B, Parlakian A, Besson V, Gomes ER, Marazzi G, and Sassoon DA (2010). Identification and characterization of a non-satellite cell muscle resident progenitor during postnatal development. Nat. Cell Biol 12, 257–266. [PubMed: 20118923]

Montarras D, Morgan J, Collins C, Relaix F, Zaffran S, Cumano A, Partridge T, and Buckingham M (2005). Direct isolation of satellite cells for skeletal muscle regeneration. Science 309, 2064–2067. [PubMed: 16141372]

Montgomery RK, Carlone DL, Richmond CA, Farilla L, Kranendonk ME, Henderson DE, Baffour-Awuah NY, Ambruzs DM, Fogli LK, Algra S, and Breault DT (2011). Mouse telomerase reverse transcriptase (mTert) expression marks slowly cycling intestinal stem cells. Proc. Natl. Acad. Sci. USA 108, 179–184. [PubMed: 21173232]

Murphy MM, Lawson JA, Mathew SJ, Hutcheson DA, and Kardon G (2011). Satellite cells, connective tissue fibroblasts and their interactions are crucial for muscle regeneration. Development 138, 3625–3637. [PubMed: 21828091]

Nguyen PD, Gurevich DB, Sonntag C, Hersey L, Alaei S, Nim HT, Siegel A, Hall TE, Rossello FJ, Boyd SE, et al. (2017). Muscle Stem Cells Undergo Extensive Clonal Drift during Tissue Growth via Meox1-Mediated Induction of G2 Cell-Cycle Arrest. Cell Stem Cell 21, 107–119.e6. [PubMed: 28686860]

Nishijo K, Hosoyama T, Bjornson CR, Schaffer BS, Prajapati SI, Bahadur AN, Hansen MS, Blandford MC, McCleish AT, Rubin BP, et al. (2009). Biomarker system for studying muscle, stem cells, and cancer in vivo. FASEB J. 23, 2681–2690. [PubMed: 19332644]

Pallafacchina G, François S, Regnault B, Czarny B, Dive V, Cumano A, Montarras D, and Buckingham M (2010). An adult tissue-specific stem cell in its niche: a gene profiling analysis of in vivo quiescent and activated muscle satellite cells. Stem Cell Res. (Amst.) 4, 77–91.

Pani L, Horal M, and Loeken MR (2002). Rescue of neural tube defects in Pax-3-deficient embryos by p53 loss of function: implications for Pax-3-dependent development and tumorigenesis. Genes Dev. 16, 676–680. [PubMed: 11914272]

Park D, Spencer JA, Koh BI, Kobayashi T, Fujisaki J, Clemens TL, Lin CP, Kronenberg HM, and Scadden DT (2012). Endogenous bone marrow MSCs are dynamic, fate-restricted participants in bone maintenance and regeneration. Cell Stem Cell 10, 259–272. [PubMed: 22385654]

Relaix F, Rocancourt D, Mansouri A, and Buckingham M (2005). A Pax3/Pax7-dependent population of skeletal muscle progenitor cells. Nature 435, 948–953. [PubMed: 15843801]

Relaix F, Montarras D, Zaffran S, Gayraud-Morel B, Rocancourt D, Tajbakhsh S, Mansouri A, Cumano A, and Buckingham M (2006). Pax3 and Pax7 have distinct and overlapping functions in adult muscle progenitor cells. J. Cell Biol 172, 91–102. [PubMed: 16380438]

Rocheteau P, Gayraud-Morel B, Siegl-Cachedenier I, Blasco MA, and Tajbakhsh S (2012). A subpopulation of adult skeletal muscle stem cells retains all template DNA strands after cell division. Cell 148, 112–125. [PubMed: 22265406]

Rodriguez-Fraticelli AE, Wolock SL, Weinreb CS, Panero R, Patel SH, Jankovic M, Sun J, Calogero RA, Klein AM, and Camargo FD (2018). Clonal analysis of lineage fate in native haematopoiesis. Nature 553, 212–216. [PubMed: 29323290]

Rogakou EP, Pilch DR, Orr AH, Ivanova VS, and Bonner WM (1998). DNA double-stranded breaks induce histone H2AX phosphorylation on serine 139. J. Biol. Chem 273, 5858–5868. [PubMed: 9488723]

Ryall JG, Dell'Orso S, Derfoul A, Juan A, Zare H, Feng X, Clermont D, Koulnis M, Gutierrez-Cruz G, Fulco M, and Sartorelli V (2015). The NAD(+)-dependent SIRT1 deacetylase translates a metabolic switch into regulatory epigenetics in skeletal muscle stem cells. Cell Stem Cell 16, 171–183. [PubMed: 25600643]

Sacco A, Doyonnas R, Kraft P, Vitorovic S, and Blau HM (2008). Self-renewal and expansion of single transplanted muscle stem cells. Nature 456, 502–506. [PubMed: 18806774]

Sambasivan R, Yao R, Kissenpfennig A, Van Wittenberghe L, Paldi A, Gayraud-Morel B, Guenou H, Malissen B, Tajbakhsh S, and Galy A (2011). Pax7-expressing satellite cells are indispensable for adult skeletal muscle regeneration. Development 138, 3647–3656. [PubMed: 21828093]

Schneider A, Zhang Y, Guan Y, Davis LS, and Breyer MD (2003). Differential, inducible gene targeting in renal epithelia, vascular endothelium, and viscera of Mx1Cre mice. Am. J. Physiol. Renal Physiol 284, F411–F417. [PubMed: 12529277]

Shea KL, Xiang W, LaPorta VS, Licht JD, Keller C, Basson MA, and Brack AS (2010). Sprouty1 regulates reversible quiescence of a self-renewing adult muscle stem cell pool during regeneration. Cell Stem Cell 6, 117–129. [PubMed: 20144785]

Simsek T, Kocabas F, Zheng J, Deberardinis RJ, Mahmoud AI, Olson EN, Schneider JW, Zhang CC, and Sadek HA (2010). The distinct metabolic profile of hematopoietic stem cells reflects their location in a hypoxic niche. Cell Stem Cell 7, 380–390. [PubMed: 20804973]

Sipkins DA, Wei X, Wu JW, Runnels JM, Côté D, Means TK, Luster AD, Scadden DT, and Lin CP (2005). In vivo imaging of specialized bone marrow endothelial microdomains for tumour engraftment. Nature 435, 969–973. [PubMed: 15959517]

Smith LM, Anderson JR, Qualman SJ, Crist WM, Paidas CN, Teot LA, Pappo AS, Link MP, Grier HE, Wiener ES, et al. (2001). Which patients with microscopic disease and rhabdomyosarcoma experience relapse after therapy? A report from the soft tissue sarcoma committee of the children's oncology group. J. Clin. Oncol 19, 4058–4064. [PubMed: 11600608]

Southard S, Low S, Li L, Rozo M, Harvey T, Fan CM, and Lepper C (2014). A series of Cre-ER(T2) drivers for manipulation of the skeletal muscle lineage. Genesis 52, 759–770. [PubMed: 24844572]

Sun J, Ramos A, Chapman B, Johnnidis JB, Le L, Ho YJ, Klein A, Hofmann O, and Camargo FD (2014). Clonal dynamics of native haematopoiesis. Nature 514, 322–327. [PubMed: 25296256]

Tian H, Biehs B, Warming S, Leong KG, Rangell L, Klein OD, and de Sauvage FJ (2011). A reserve stem cell population in small intestine renders Lgr5-positive cells dispensable. Nature 478, 255–259. [PubMed: 21927002]

Tierney MT, Stec MJ, Rulands S, Simons BD, and Sacco A (2018). Muscle Stem Cells Exhibit Distinct Clonal Dynamics in Response to Tissue Repair and Homeostatic Aging. Cell Stem Cell 22, 119–127.e3. [PubMed: 29249462]

Vahidi Ferdousi L, Rocheteau P, Chayot R, Montagne B, Chaker Z, Flamant P, Tajbakhsh S, and Ricchetti M (2014). More efficient repair of DNA double-strand breaks in skeletal muscle stem cells compared to their committed progeny. Stem Cell Res. (Amst.) 13 (3 Pt A), 492–507.

Velasco-Hernandez T, Säwén P, Bryder D, and Cammenga J (2016). Potential Pitfalls of the Mx1-Cre System: Implications for Experimental Modeling of Normal and Malignant Hematopoiesis. Stem Cell Reports 7, 11–18. [PubMed: 27373927]

Verovskaya E, Broekhuis MJ, Zwart E, Ritsema M, van Os R, de Haan G, and Bystrykh LV (2013). Heterogeneity of young and aged murine hematopoietic stem cells revealed by quantitative clonal analysis using cellular barcoding. Blood 122, 523–532. [PubMed: 23719303]

Ward JF (1985). Biochemistry of DNA lesions. Radiat. Res. Suppl 8, S103–S111. [PubMed: 3867077]

Wilson A, Laurenti E, Oser G, van der Wath RC, Blanco-Bose W, Jaworski M, Offner S, Dunant CF, Eshkind L, Bockamp E, et al. (2008). Hematopoietic stem cells reversibly switch from dormancy to self-renewal during homeostasis and repair. Cell 135, 1118–1129. [PubMed: 19062086]

Yang G, Li Y, Nishimura EK, Xin H, Zhou A, Guo Y, Dong L, Denning MF, Nickoloff BJ, and Cui R (2008). Inhibition of PAX3 by TGF-beta modulates melanocyte viability. Mol. Cell 32, 554–563. [PubMed: 19026785]

Zalc A, Rattenbach R, Auradé F, Cadot B, and Relaix F (2015). Pax3 and Pax7 play essential safeguard functions against environmental stress-induced birth defects. Dev. Cell 33, 56–66. [PubMed: 25800090]

Highlights

- Mx1-Cre marks a subset of label-retaining muscle stem cells (SCs)
- Mx1-Cre^{+} muscle stem cells function as a radiotolerant reserve SC population
- Pax3 is enriched and required for clonal expansion of reserveSCs after radiation
- ROS levels endow radiotolerance of reserve SCs

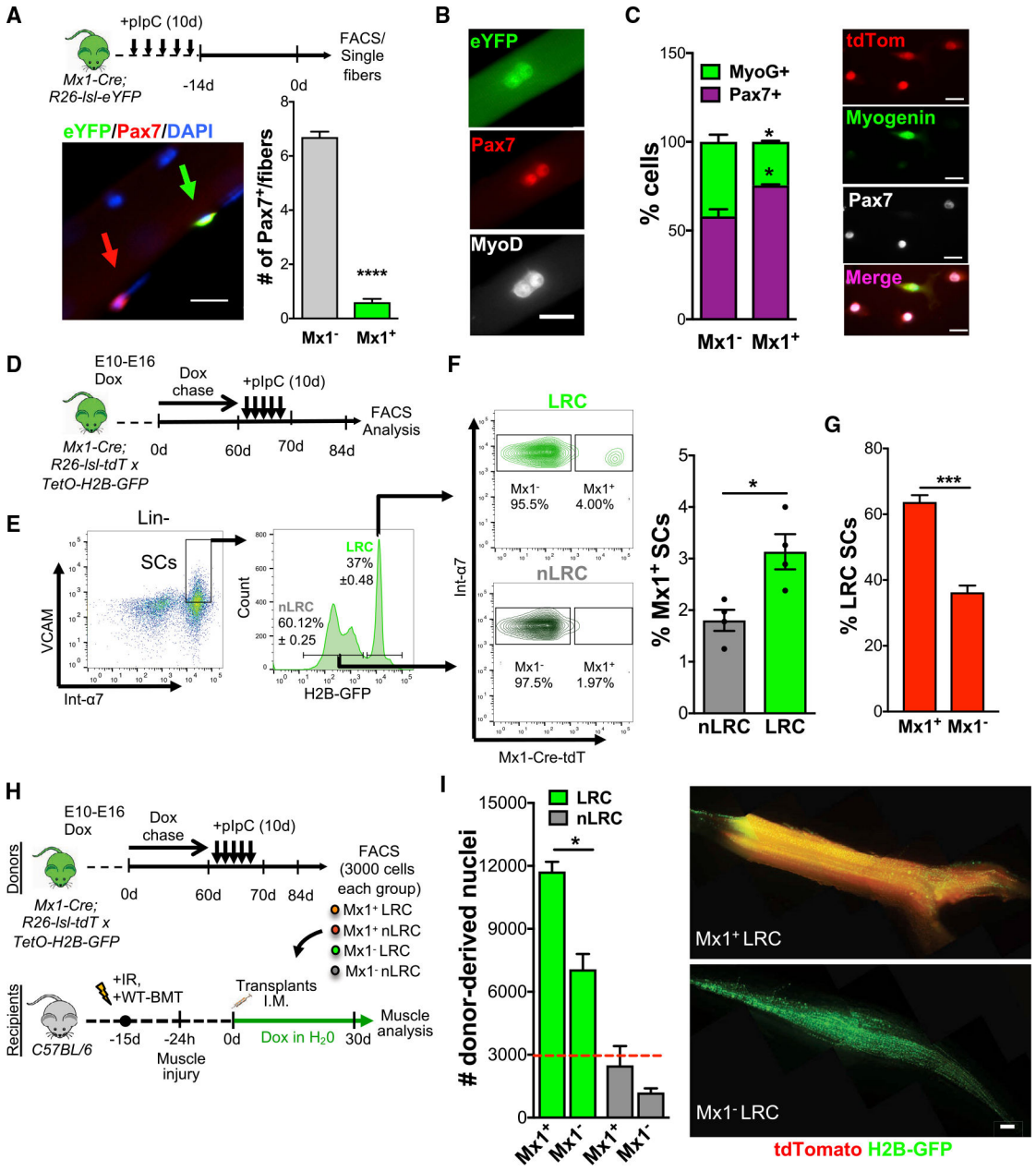

Figure 1. Mx1-Cre Marks a Subset of Pax7$^+$ SCs

(A) Scheme of pIpC injection, FACS, and single muscle fiber harvesting for *Mx1-Cre;R26-lsl-eYFP* mice (top). Single muscle fiber stained for eYFP and Pax7 (left) and number of Mx1$^+$ and Mx1$^-$Pax7$^+$ SCs/muscle fiber (right) is shown. Mx1$^+$ (green arrow) and Mx1$^-$(red arrow) SCs (n = 4−6 mice) are shown.

(B) Mx1$^+$ SCs on single muscle fibers after 48 h in culture stained for eYFP, Pax7, and MyoD.

(C) Percentage of Pax7$^+$ and myogenin$^+$ cells from *Mx1-Cre;R26-lsl-tdT* mice after 4 days in culture (2,000 cells total; n = 3 mice; left) and representative image (right).

(D) Embryonic Dox labeling (E10–E16), chase, and pIpC injection in *Mx1-Cre;R26-lsl-tdT* mice crossed with *TetO-H2B-GFP*.

(E) FACS plots from *Mx1-Cre;R26-lsl-tdT.TetO-H2B-GFP* mice. Percentage of LRCs and nLRCs is shown.

(F) FACS plots (left) and percentage of $Mx1^+$ LRC/nLRC (right) from *Mx1-Cre;R26-lsl-tdT.TetO-H2B-GFP* mice (n = 4 mice).

(G) Percentage of LRCs within $Mx1^+$ and $Mx1^-$SCs (n = 4 mice).

(H) Schematic of donor $Mx1^+$ and Mx1 LRC/nLRC derived from embryonically Dox-labeled, chased, and pIpC-treated *Mx1-Cre;R26-lsl-tdT.TetO-H2B-GFP* mice, transplanted into WT host exposed to whole-body IR, WT-BMT, and $BaCl_2$-muscle injured. Dox water was given to the host during regeneration.

(I) Number of $Mx1^+$ and $Mx1^-$LRC/nLRC donor-derived nuclei per muscle. Red dashed line represents number of transplanted cells (left). Images of transplanted muscle from $Mx1^+$ and $Mx1^-$ LRCs (right; n = 3 mice) are shown.

Data are presented as mean ± SEM in (A), (F), (G), and (I), and as SD in (C); $^{****}p < 0.0001$, $^{***}p < 0.001$, $^{*}p < 0.05$. Scale bars, 20 μm in (A)–(C) and 500 μm (E). DAPI was used for nuclear staining. See also Figure S1.

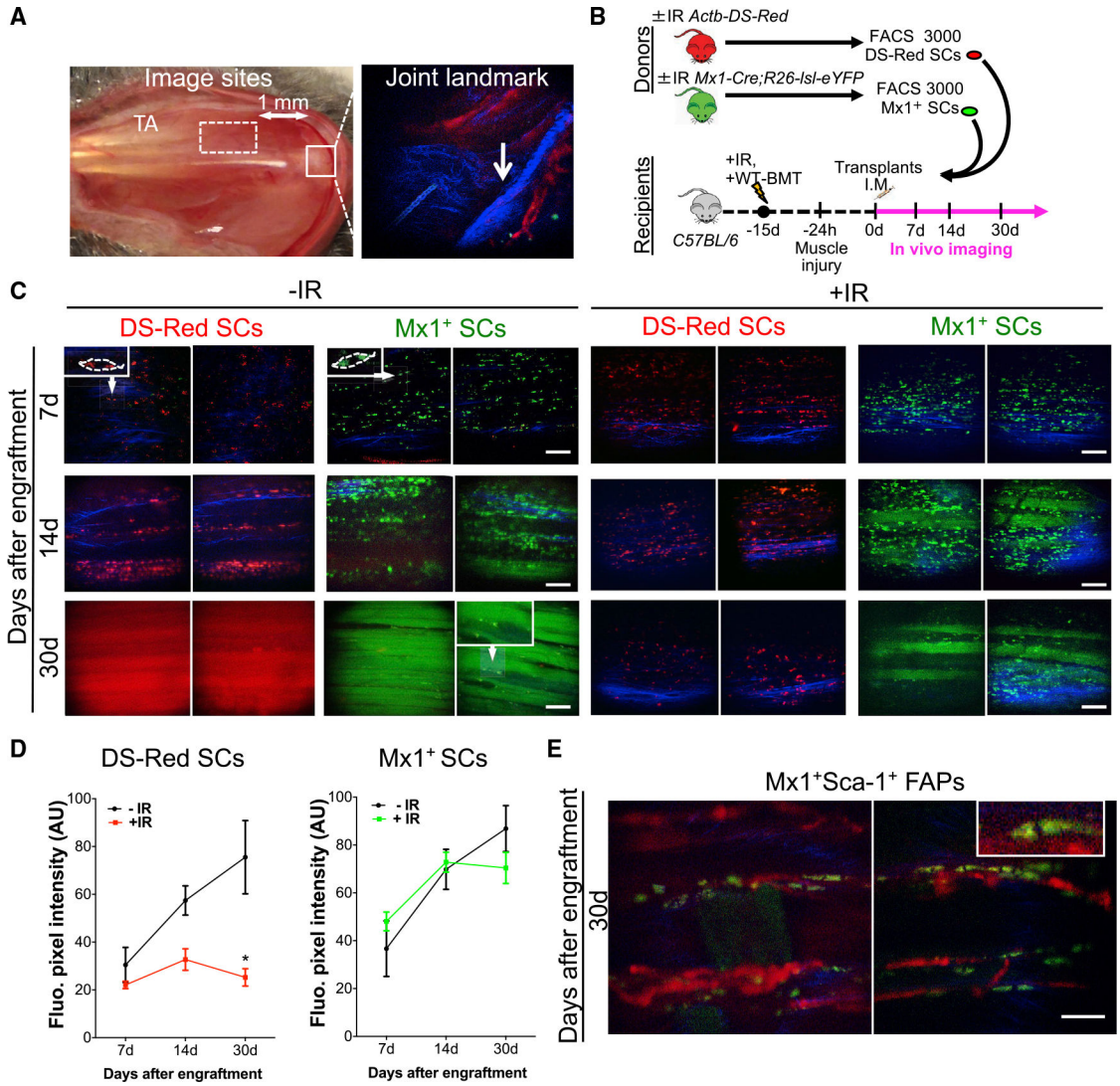

Figure 2. Mx1-Cre^{+} SCs Retain Stem Cell Potential after Irradiation

(A) Imaging site of TA muscle (dashed square) that is ~1 mm apart from tibial head (solid square) is shown (left). Bone collagen (blue) and vasculature-using quantum-dot labeling (red) are shown.

(B) Schematic of transplantation and sequential imaging of FACS sorted DS-Red and Mx1^{+} SCs from ±IR *Actb-DS-Red* and ±IR *Mx1-Cre;R26-lsl-eYFP* donor mice into WT mice exposed to 9 Gy whole-body IR, WT-BMT, and $BaCl_2$ muscle injury

(C) Sequential images of pre-IR and $BaCl_2$-injured muscles transplanted with 3,000 Mx1^{+} SCs (green) or DS-Red SCs (red) from ±IR donor mice at 7, 14, and 30 days after engraftment. Collagen fibrils are in blue. High magnification of engrafted cells is in top left corner.

(D) Mean fiber fluorescence pixel intensity (a.u.) from z stack reconstructions in recipient mice transplanted with DS-Red SCs and Mx1^{+} SCs.

(E) *In vivo* imaging of injured muscles 30 days after engraftment of 3,000 $Mx1^{+}Sca1^{+}$ FAPs. Top right corner shows interstitial $Mx1^{+}Sca1^{+}$ cells outside the muscle fibers in the perivascular space (quantum-dot labeling; red).

Data are presented as mean ± SD; *$p < 0.05$. Scale bars, 100 μm. DAPI was used for nuclear staining. See also Figure S2.

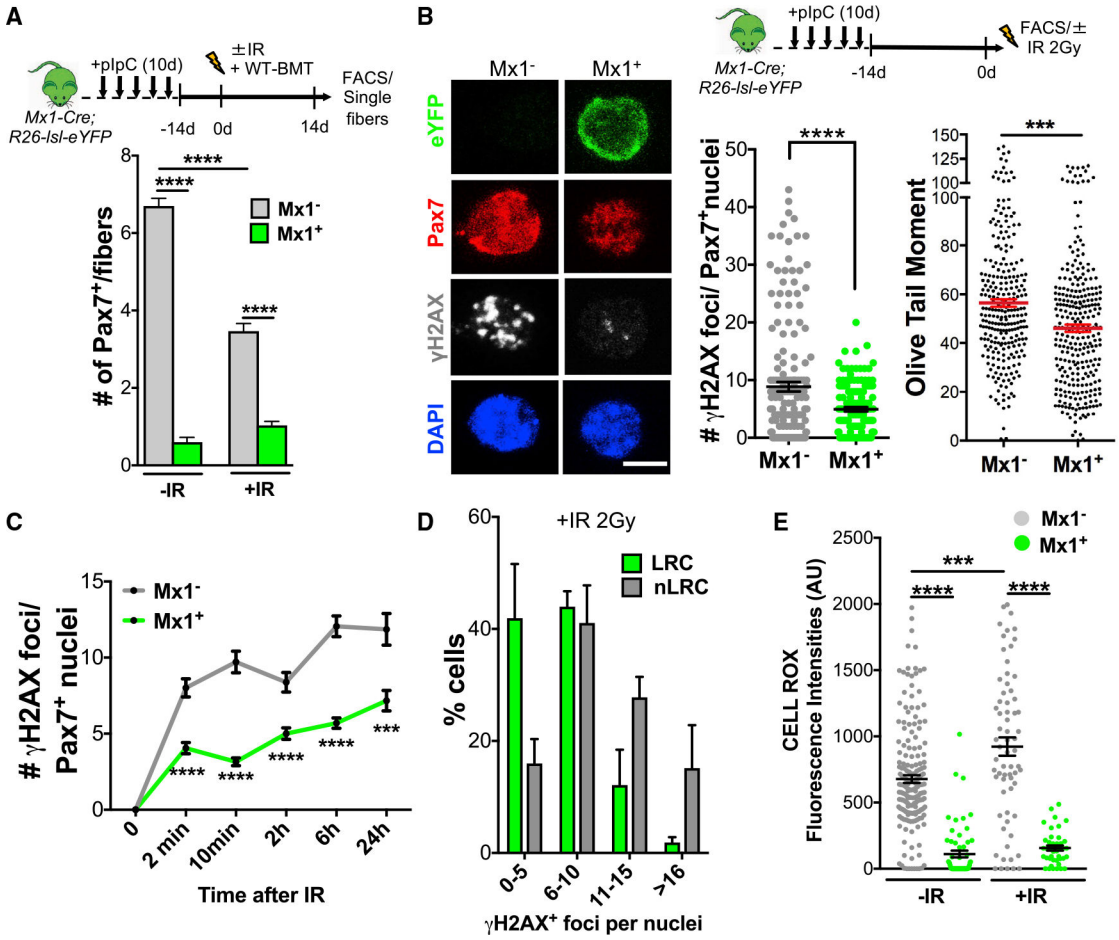

Figure 3. Mx1-Cre^{+} SCs Are Radiotolerant

(A) Scheme of pIpC injection for *Mx1-Cre;R26-lsl-eYFP* mice, IR, WT-BMT, FACS, and muscle fiber harvesting (top). Number of Mx1^{+} and Mx1^{-}Pax7^{+} SCs/fiber from ±IR *Mx1-Cre;R26-lsl-eYFP* mice (n = 4–6 mice; bottom).

(B) Schematic of pIpC injection of *Mx1-Cre;R26-lsl-eYFP*, FACS, and *in vitro* IR of SCs (top). +IR Mx1 and Mx1^{+} SCs stained for YFP, Pax7, and γH2AX (left) are shown. Number of γH2AX^{+} foci per Pax7^{+} nuclei 10 min after *in vitro* IR exposure is shown (2 Gy; 130 → 174 cells total; n = 3 mice; middle). Olive tail moment 10 min after 2 Gy IR is shown (150 → 300 cells per condition, n = 3; right).

(C) Time course of γH2AX^{+} foci per Pax7^{+} nuclei after IR (100 → 225 cells each time point; n = 3 mice).

(D) Binned ranges of γH2AX^{+} foci per nuclei in FACS sorted LRC and nLRC 10 min after *in vitro* IR (2 Gy).

(E) Mean cell ROX fluorescence intensity (a.u.) 60 min after 2 Gy IR (50 → 188 cells; n = 3).

Data are presented as mean ± SEM in (A)–(C) and (E), and as SD in (D); $^{**}p < 0.01$; $^{***}p < 0.001$; $^{****}p < 0.0001$. Scale bar, 5 μm. DAPI was used for nuclear staining. See also Figure S3.

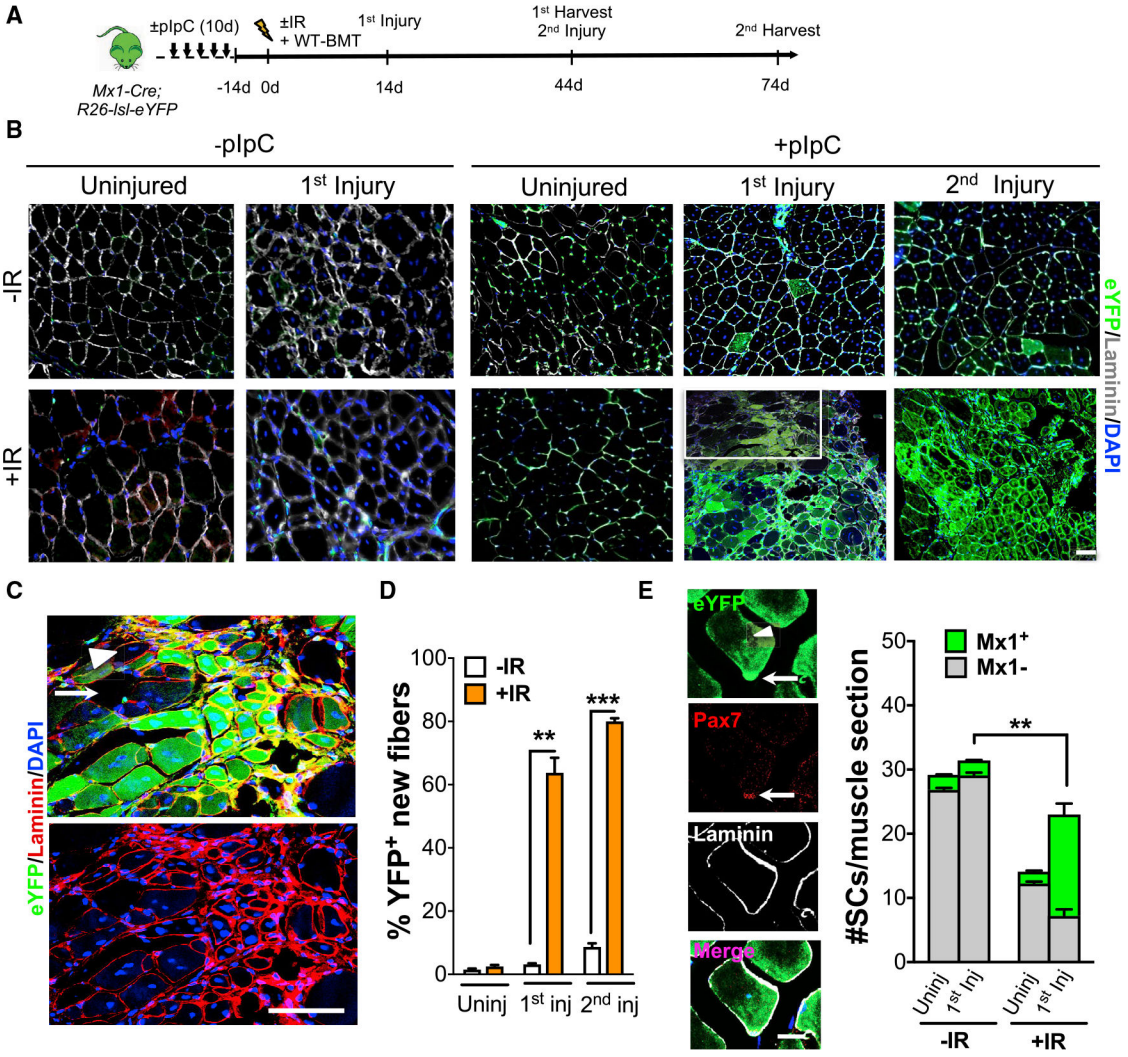

Figure 4. Mx1-Cre^{+} SCs Function as Reserve Muscle Stem Cells

(A) Scheme of pIpC administration of *Mx1-Cre;R26-lsl-eYFP* mice, prior to IR, WT-BMT, and multiple rounds of muscle injury.

(B) Muscle sections from uninjured and injured muscles ±pIpC and ±IR. Muscle sections stained for eYFP and laminin. Inset in +IR 1st injury is described in (C).

(C) High magnification of regenerating muscle (from inset in B) after 1st injury and IR. White arrowhead shows a rare YFP regenerated muscle fiber, surrounded by YFP^{+} regenerating muscle fibers. Non-regenerating fibers have undetectable levels of YFP (white arrow).

(D) Percentage of YFP^{+} fibers in uninjured, primary, and secondary injured muscle in ±IR conditions.

(E) Central-nucleated Mx1^{+} muscle fiber (arrowhead) and Mx1^{+} SCs (white arrow) under the basal lamina 30 days after primary injury, detected by anti-GFP, anti-laminin, and anti-Pax7 staining (left). Number of SCs/muscle section (n = 3 mice) from uninjured and 1st injury from ±IR (right) is shown.

Data are presented as mean ± SEM in (D), and as SD in (E); $^{**}p < 0.01$; $^{***}p < 0.001$. Scale bars, 50 μm in (B), 100 μm in (C), and 10 μm in (E). DAPI was used for nuclear staining. See also Figure S4.

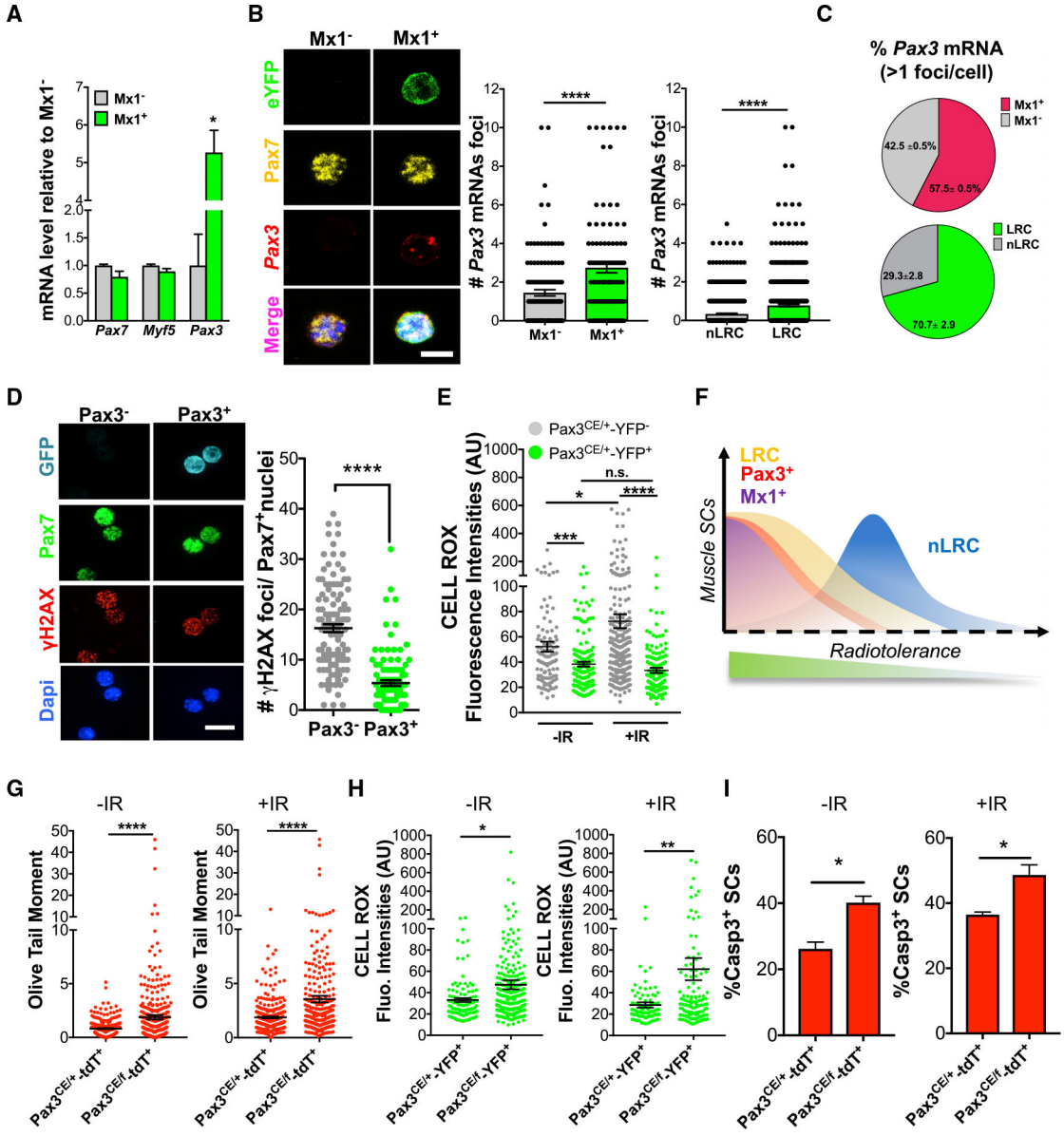

Figure 5. Pax3 Is Enriched in Mx1-Cre^{+} SCs

(A) Transcript levels of *Pax7*, *Myf5*, and *Pax3* in freshly isolated Mx1^{+} and Mx1^{-} SCs (n = 3).

(B) Confocal images of RNA FISH for *Pax3* (red) combined with immunohistochemical detection of eYFP (green) and Pax7 (yellow; left). Number of *Pax3* mRNA foci in Mx1^{+}/Mx1^{-} SCs (100 → 130 cells; n = 2; middle) and LRC/nLRCs (518 → 517 cells; n = 2; left) is shown.

(C) Percentage of *Pax3*$^{+}$ mRNA foci in Mx1^{+}/Mx1^{-} SCs (top) and LRC/nLRCs (bottom) from (B).

(D) Confocal images of Pax3^{-} and Pax3^{+} SCs from *Pax3*$^{GFP/+}$ mice stained for GFP, Pax7, and γH2AX (left). Number of γH2AX^{+} foci per Pax7^{+} nuclei 10 min after *in vitro* +IR (2 Gy; n = 4 mice; right) is shown.

(E) Mean cell ROX fluorescence intensity (a.u.) before and 60 min after 2 Gy IR (103 → 256 cells; n = 3).
(F) Model of radiotolerance based on γH2AX DNA damage analysis across SC populations. Radiotolerance operates as a continuum with $Mx1^{+}$, $Pax3^{+}$, and LRC at one end and nLRC at the other end of the damage distribution.
(G) Olive tail moment from $Pax3^{CE/+}$-tdT^{+} and $Pax3^{CE/f}$-tdT^{+} SCs in −IR and +IR (10 min after 2 Gy IR; 269 → 374 cells; n = 3).
(H) Mean cell ROX fluorescence intensity (a.u.) of FACS sorted $Pax3^{CE/+}$-YFP^{+} and $Pax3^{CE/f}$-YFP^{+} SCs in −IR and +IR (60 min after 2 Gy IR; 100 → 267 cells; n = 3).
(I) Percentage of caspase 3^{+} SCs 48 h after +IR *in vitro* (n = 3).
Data are presented as mean ± SEM in (B), (D), (E), and (G)–(I), and as SD in (A); $^{****}p < 0.0001$; $^{***}p < 0.001$; $^{**}p < 0.01$; $^{*}p < 0.05$. Scale bars, 5 μm. DAPI was used for nuclear staining. See also Figure S5.

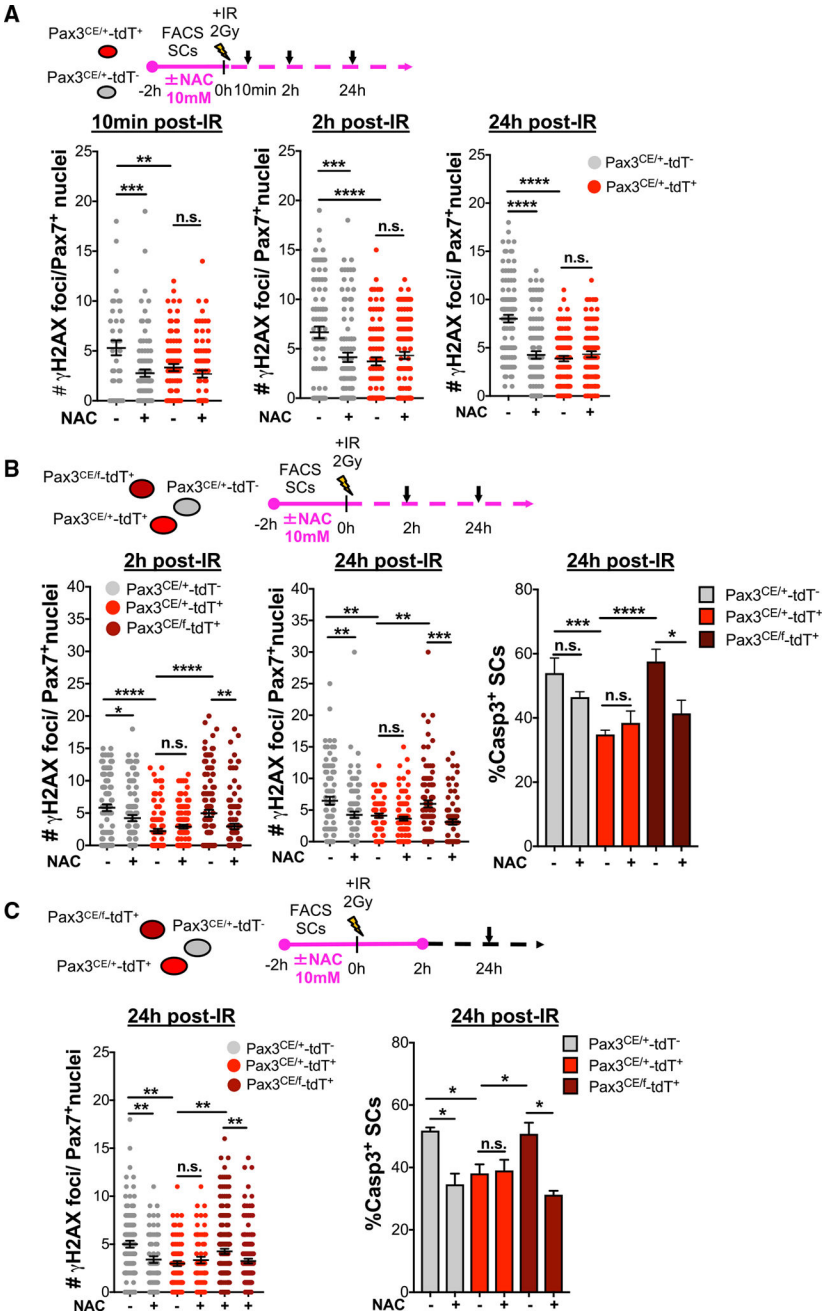

Figure 6. Inhibition of ROS Promotes Tolerance and Survival in Radiosensitive SCs

(A) Schematic of Pax3$^{CE/+}$-tdT^{+} and Pax3$^{CE/+}$-tdT SCs treated with or without NAC up to 24 h post-IR (top) and number of γH2AX^{+} foci per Pax7^{+}nuclei at 10 min, 2 h, and 24 h post-IR (n = 2; bottom).

(B) Schematic of Pax3$^{CE/+}$-tdT^{+}, Pax3$^{CE/+}$-tdT$^{–}$, and Pax3$^{CE/f}$-tdT^{+} SCs treated with or without NAC up to 24 h post-IR (top). Number of γH2AX^{+} foci per Pax7^{+} nuclei at 2 h and 24 h post-IR and percentage of caspase3^{+} SCs after 24 h in culture (n = 2) is shown.

(C) Schematic of Pax3$^{CE/+}$-tdT^{+}, Pax3$^{CE/+}$-tdT^{-}, and Pax3$^{CE/f}$-tdT^{+} SCs treated with or without NAC up to 2 h post-IR (top). Number of γH2AX^{+} foci per Pax7^{+} nuclei and percentage of caspase3^{+} SCs after 24 h in culture with or without NAC (n = 2) is shown. Data are presented as mean ± SEM; $^{****}p < 0.0001$; $^{***}p < 0.001$; $^{**}p < 0.01$; $^{*}p < 0.05$; n.s., not significant. See also Figure S6.

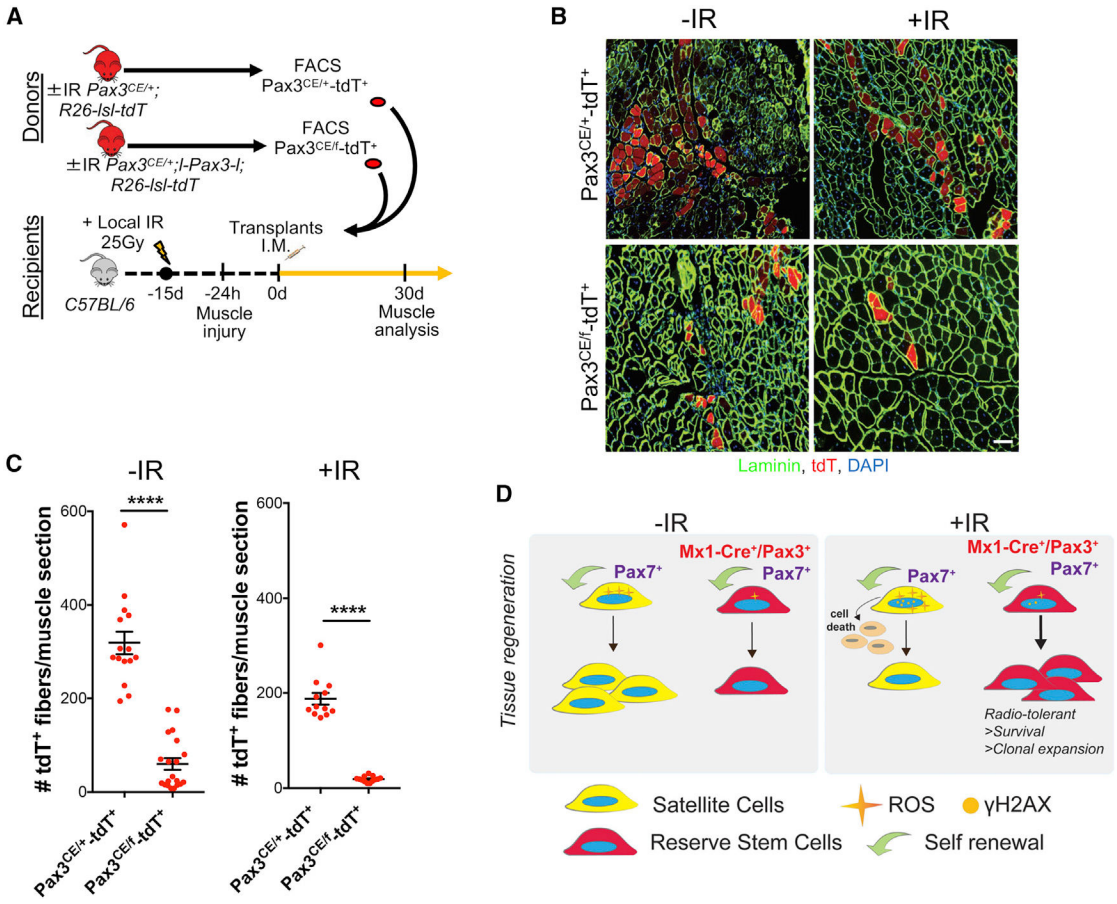

Figure 7. Pax3 Is Required for RSC Clonal Expansion after Transplantation

(A) Schematic of 3,000 $Pax3^{+}$ SCs from ±IR $Pax3^{CE/+}$-tdT^{+} and $Pax3^{CE/f}$-tdT^{+} donor mice transplanted into locally IR (24 Gy) and $BaCl_2$-injured muscle of WT recipient mice.

(B) Image of muscle cross-section from transplanted ±IR $Pax3^{CE/+}$-tdT^{+} and $Pax3^{CE/f}$-tdT^{+} SCs (from A). Muscle stained with anti-laminin (green) is shown.

(C) Number of tdT^{+} donor-derived fibers/muscle section from transplanted ±IR $Pax3^{CE/+}$-tdT^{+} and $Pax3^{CE/f}$-tdT^{+} SCs (from A; n = 13 → 20 sections across 1 mm of TA muscle; n = 3 mice).

(D) Model of radiotolerant $Mx1\text{-}Cre^{+}/Pax3^{+}/Pax7^{+}$ RSCs capable of clonal expansion during tissue regeneration upon radiation stress.

Data are presented as mean ± SEM; $^{****}p < 0.0001$. Scale bar, 100 μm. DAPI was used for nuclear staining.

KEY RESOURCES TABLE

REAGENT or RESOURCE	SOURCE	IDENTIFIER
Antibodies		
Anti- VCAM1/CD106 (MVCAMA(429)) Biotin	Novus Bio	Cat#NB100-63333 AB_959528
Mouse CD106/VCAM1 PE	Invitrogen	Cat#RMCD10604 AB_2556576
Alpha 7 integrin 647 Clone:R2F2	Ab Labs	Cat#67-0010-05
APC-Cy7 Rat anti mouse Ly-6A/E Clone:D7	BD Pharmigen	Cat#560654 AB_1727552
PE-Cy7 Rat anti mouse CD31 Clone: 390	BD Pharmigen	Cat#561410AB_10612003
PE-Cy7 Rat anti mouse CD45 Clone: 30-F11	BD Pharmigen	Cat#552848 AB_394489
PE-anti mouse CD140a Clone:APA5	Biolegend	Cat#135905 AB_1953268
Brilliant Violet 421 Streptavidin	BioLegend	Cat#405226
PE anti mouse CD105 Clone: MJ7/18	BioLegend	Cat#120407 AB_1027701
Propidium Iodide PI solution	Sigma-Aldrich	Cat#P4862
7-AAD	BD Parmingen	Cat#51-68981E
Pax7-c	Developmental Studies Hybridoma Bank	http://dshb.biology.uiowa.edu/PAX7
MyoD(M-318)	Santa Cruz Biotechnology	Cat#sc-760 AB_2148870
Myogenin (M-225)	Santa Cruz Biotechnology	Cat#sc-576 AB_2148908
GFP (chicken)	Aves Labs	Cat#GFP-1020 AB_10000240
GFP (rabbit)	Thermo Fisher	Cat#A11122 AB_221569
MHC (rabbit)	Sigma-Aldrich	Cat#M7659
Laminin (rabbit)	Abeam	Cat#ab11575AB_298179
Laminin (chicken)	Abeam	Cat#ab14055 AB_300883
Ki67 (rabbit)	Abeam	Cat#ab16667 AB_302459
Cleaved Caspase 3	Cell Signaling	Cat#9661S AB_2341188
p-Histone H2AX (S139)	Cell Signaling	Cat#9718S AB_2118009
Brdu (rat)	Abeam	Cat#ab6326 AB_305426
Chemicals, Peptides, and Recombinant Proteins		
N-Acetyl-L-cysteine	Sigma-Aldrich	Cat#7250
Tamoxifen	Sigma-Aldrich	Cat#T5648
Polyinosinic-polycytidylic acid sodium salt	Sigma-Aldrich	Cat#P1530
Doxycycline hyclate	Sigma-Aldrich	Cat#D9891
5-Bromo-2′deoxyuridine	Sigma-Aldrich	Cat#B5002
Critical Commercial Assays		
CellROX DeepRed Reagent, for oxidative stress detection	Thermo Fisher	Cat# C10422
Cellular senescence assay kit	EMD Mlllipore	Cat# KAA002
RNAscope® Multiplex Fluorescent Reagent Kit V2	ACD	Cat# 323100
TUNEL Andy Fluor 647 Apoptosis Detection Kit	GeneCopoeia	Cat# A052
CometAssay® Kit (25 × 2 well slides)	Trevigen	Cat# 4250–050-K
Experimental Models: Organisms/Strains		
Mouse C57BL/6	Jackson Laboratories	Cat#000664
Mouse B6.Cg-Tg(Mx1-cre)1Cgn/J	Jackson Laboratories	Cat#003556
Mouse Pax3$^{tm1.1(cre/ERT2)Lepr}$/J	Jackson Laboratories	Cat#025663

REAGENT or RESOURCE	SOURCE	IDENTIFIER
Mouse B6.129X1-Gt(ROSA)26Sor$^{tm1(EYFP)Cos}$/J	Jackson Laboratories	Cat# 006148
Mouse Actb-DSred. T3	Jackson Laboratories	Cat#005441
Mouse B6.Cg-Gt(ROSA)26Sor$^{tm9(CAG-tdTomato)Hze}$/J	Jackson Laboratories	Cat#007909
Mouse Pax7-CreER™	Nishijo et al., 2009	N/A
Mouse Pax3$^{GFP/+}$	Relaix et al., 2005	N/A
Mouse loxp-Pax3-loxp	Koushik et al., 2002	N/A
Mouse TetO-H2B-GFP	Foudi et al., 2009	N/A
Oligonucleotides		
Pax7 RTqPCR forward	GTGGAATCAGAACCCGACCTC	N/A
Pax7 RTqPCR reverse	GTAGTGGGTCCTCTCAAAGGC	N/A
Myf5 RTqPCR forward	ATTACAGCCTGCCGGGACAGAG	N/A
Myf5 RTqPCR reverse	GCAATCCAAGCTGGACACGGAG	N/A
Pax3 RTqPCR forward	CGAGAGAACCCACTACCCAGAC	N/A
Pax3 RTqPCR reverse	CTCCAGCTTGTTTCCTCCATCTTG	N/A
GAPDH RTqPCR forward	GGCAAAGTGGAGATTGTTGC	N/A
GAPDH RTqPCR reverse	AATTTGCCGTGAGTGGAGTC	N/A
RNA scope probe Mm-Pax3-C2	ACD	Cat#455801-C2
Software and Algorithms		
Graphpad-Prism Software		https://www.graphpad.com
FlowJow software		https://www.flowjo.com/
CometScore	TriTekCorp	N/A